nature communications

Article

https://doi.org/10.1038/s41467-024-51828-2

# RAS-ON inhibition overcomes clinical resistance to KRAS G12C-OFF covalent blockade

Received: 21 November 2023

Accepted: 20 August 2024

Published online: 30 August 2024

Check for updates

Marie-Julie Nokin[1,12,13], Alessia Mira[2,13], Enrico Patrucco[2], Biagio Ricciuti[3], Sophie Cousin[4], Isabelle Soubeyran[5], Sonia San José[1,6], Serena Peirone[7,8], Livia Caizzi[8], Sandra Vietti Michelina[2], Aurelien Bourdon[5], Xinan Wang[3], Daniel Alvarez-Villanueva[9], María Martínez-Iniesta[9], August Vidal[9], Telmo Rodrigues[10], Carmen García-Macías[10], Mark M. Awad[3], Ernest Nadal[11], Alberto Villanueva[9,11], Antoine Italiano[4] ✉, Matteo Cereda[7,8] ✉, David Santamaría[1,6] ✉ & Chiara Ambrogio[2] ✉

Selective KRAS$^{G12C}$ inhibitors have been developed to covalently lock the oncogene in the inactive GDP-bound state. Two of these molecules, sotorasib and adagrasib, are approved for the treatment of adult patients with KRAS$^{G12C}$-mutated previously treated advanced non-small cell lung cancer. Drug treatment imposes selective pressures leading to the outgrowth of drug-resistant variants. Mass sequencing from patients' biopsies identified a number of acquired *KRAS* mutations -both in *cis* and in *trans*- in resistant tumors. We demonstrate here that disease progression in vivo can also occur due to adaptive mechanisms and increased KRAS-GTP loading. Using the preclinical tool tri-complex KRAS$^{G12C}$-selective covalent inhibitor, RMC-4998 (also known as RM-029), that targets the active GTP-bound (ON) state of the oncogene, we provide a proof-of-concept that the clinical stage KRAS$^{G12C}$(ON) inhibitor RMC-6291 alone or in combination with KRAS$^{G12C}$(OFF) drugs can be an alternative potential therapeutic strategy to circumvent resistance due to increased KRAS-GTP loading.

*KRAS* is the most frequent human oncogene taking into account both its high prevalence and its broad cancer distribution[1]. This has led to tremendous efforts in the last decades aimed at designing clinically relevant treatments that have nonetheless invariably produced disappointing results. Medicinal chemistry approaches based on the pioneering work by Shokat and colleagues[2] have resulted in the development of two specific inhibitors of the *KRAS$^{G12C}$* allele—sotorasib[3,4] and adagrasib[5,6]. These drugs bind to a switch II region pocket accessible when KRAS is in the GDP-bound inactive state (RAS(OFF) inhibitors). Upon binding, both compounds covalently

[1]INSERM U1312, University of Bordeaux, IECB, Pessac, France. [2]Department of Molecular Biotechnology and Health Sciences, Molecular Biotechnology Center, University of Torino, Torino, Italy. [3]Department of Medical Oncology, Dana–Farber Cancer Institute, Boston, MA, USA. [4]Department of Medical Oncology, Institut Bergonié, Bordeaux, France. [5]Department of Biopathology, Institut Bergonié, Bordeaux, France. [6]Molecular Mechanisms of Cancer Program, Centro de Investigación del Cáncer, CSIC-Universidad de Salamanca, Salamanca, Spain. [7]Department of Biosciences, Università degli Studi di Milano, Via Celoria 26, Milan, Italy. [8]Italian Institute for Genomic Medicine, c/o IRCCS, Str. Prov. le 142, km 3.95, Candiolo, Torino, Italy. [9]Chemoresistance and Predictive Factors Group, Program Against Cancer Therapeutic Resistance (ProCURE), Catalan Institute of Oncology (ICO), L'Hospitalet de Llobregat, Barcelona, Spain. [10]Comparative Pathology Unit, Centro de Investigación del Cáncer, CSIC-Universidad de Salamanca, Salamanca, Spain. [11]Department of Medical Oncology, Catalan Institute of Oncology (ICO); Preclinical and Experimental Research in Thoracic Tumors (PReTT) Group, Oncobell Program, IDIBELL, L'Hospitalet, Barcelona, Spain. [12]Present address: Laboratory of Biology of Tumor and Development (LBTD), GIGA-Cancer, University of Liège, Liège, Belgium. [13]These authors contributed equally: Marie-Julie Nokin, Alessia Mira. ✉e-mail: a.italiano@bordeaux.unicancer.fr; matteo.cereda@iigm.it; d.santamaria@usal.es; chiara.ambrogio@unito.it

engage with the mutant cysteine, irreversibly locking the oncogene in its inactive form (reviewed in ref. 7). The first clinical trials investigating these agents in patients with previously treated advanced non-small cell lung cancer (NSCLC) harboring *KRAS*$^{G12C}$ mutation showed very promising results with response rates ranging between 37% and 45% and disease control rates of 81 and 96% respectively[3]. Based on these results, sotorasib[3,4] and adagrasib[5,6], were granted FDA accelerated approval. Yet, recent clinical findings highlighted that the degree of therapeutic benefit appears limited[8]. This could be in part due to the evidence that, as observed for other targeted therapies, almost all patients experiencing clinical benefit upon treatment with sotorasib or adagrasib will develop resistance[9]. Importantly, the mechanisms of resistance to KRAS inhibitors have only been clarified in less than half of NSCLC and colorectal cancer patients[7,10]. Whether resistance to therapy in the remaining fraction is due to signal adaptation engaging the RAS pathway as reported in vitro[11] remains to be elucidated. Therefore, the identification of additional resistance mechanisms and the elucidation of alternative treatments to circumvent them is an urgent medical need.

Here, we take advantage of a series of paired pre- and post-KRASi resistance patient samples, patient-derived orthoxenografts (PDOX), and cell lines generated from a patient with *KRAS*$^{G12C}$-mutant lung adenocarcinoma (LUAD) who developed resistance to sotorasib to explore potential therapeutic approaches in this setting. Our results suggest that adaptive resistance due to an increase in KRAS expression and GTP-loading with the contribution of wild-type KRAS as reported in preclinical models[11–13] is also a relevant feature in patients. Using the preclinical tool compound RMC-4998, a recently described tri-complex inhibitor that selectively targets the active GTP-bound state of KRAS$^{G12C}$[14], alone or in combination with KRAS$^{G12C}$(OFF) drugs, we also demonstrate that KRAS$^{G12C}$(ON) inhibition is a potential therapeutic strategy to re-sensitize resistant LUAD to KRAS inhibition.

## Results

### Patient, clinical record, and treatment history

A former smoker patient was diagnosed with stage IV *KRAS*$^{G12C}$ (c.*34 G > T*) positive lung adenocarcinoma (LUAD), PD-L1 <1%, and was refractory to two prior lines of therapy consisting of cisplatin plus vinorelbine and atezolizumab. The patient had a left pectoral muscle lesion, mediastinal lymphadenopathies, fourth right rib lesion, peritoneal carcinomatosis, and a series of previously irradiated stable brain metastases. The patient was therefore enrolled in the AMG-510-20170543 phase I/II clinical trial (CodeBreaK100 NCT03600883) and received AMG-510 (sotorasib, 960 mg once a day) with clinical benefit and initial stable disease within six weeks (−23% according to RECIST version 1.1). The patient was biopsied at this point (stable disease, SD), and whole-exome sequencing (WES) was performed. This was followed by a second biopsy from a progressive lesion (cycle 5, 12 weeks after initiation of treatment, progressive disease, PD) (Fig. 1A, B).

To unravel potential mechanisms of drug resistance, we carried out a comparative analysis of the WES results from the two sequential biopsies (see Methods). We found that disease progression was accompanied by altered allelic frequencies of a subset of putative driver mutations (Table 1). No secondary mutations affecting the *KRAS* oncogene were identified in addition to the original G12C driver alteration. Interestingly, the variant allelic frequency (VAF) of G12C decreased ~0.5-fold, moving from VAF = 0.89 to VAF = 0.39 status after 6 additional weeks of treatment (Fig. 1C).

### Monoclonal tumor evolution in response to treatment

To functionally evaluate the potential contribution of somatic acquired alterations to the onset and progression of the drug-resistant phenotype, we performed orthotopic implantation of the sotorasib-resistant patient-derived biopsy at tumor progression in the lung of one athymic mouse[15]. The grafted tumor was surgically extracted from the recipient mouse after two months and characterized to confirm LUAD histopathological features. In addition, the PDOX was used to derive two independent cell lines that were maintained under constant drug pressure with sotorasib (Suppl. Fig. 1).

Longitudinal sequencing obtained from samples along the entire process were compared to characterize acquired alterations potentially driving the evolution of this tumor upon treatment (Fig. 2A). We found that most of the putative driver mutations were shared across the longitudinal samples (Fig. 2B and Suppl. Fig. 2). This finding suggests the evolution of the dominant clone rather than the expansion of independent subclones upon treatment (Fig. 2B and Suppl. Data 1). Of the shared mutations, the decreased allelic frequency of *KRAS*$^{G12C}$ was confirmed in both PDOX and PDOX-derived cell lines (Fig. 2B, C). Conversely, VAF of other shared mutations, such as G476W in the tumor suppressor gene *KEAP1*, increased in response to the treatment (Fig. 2B, C). Similarly, VAF of newly acquired mutations such as *C421Y* in the tumor suppressor gene *TGFBR2* increased in the resistant biopsy, PDOX, and derived cell lines compared to the SD sample (Fig. 2B, C).

Next, we profiled the somatic copy number variations (CNVs) of the longitudinal lesions to identify driver events as a gain of oncogenes and loss of tumor suppressor genes (see Methods, Suppl. Data 2). Overall, we identified 23 known lung cancer genes that changed their allelic balance when compared to the SD biopsy (Fig. 2D and Suppl. Data 3). Amongst these genes, *KEAP1* showed a heterozygous loss in the PD biopsy. This result is in line with the increased VAF of *KEAP1* G476W (Fig. 1C), thus confirming the acquired clonality of this mutation along the longitudinal samples. Interestingly, we observed a duplication of the wild-type *KRAS* allele in the PDOX and derived cell lines (Fig. 2D). This observation could explain the decreased *KRAS*$^{G12C}$ VAF detected in the PD biopsy (Figs. 1C, 2C), although the duplication of the *KRAS* wild-type allele in this sample could not be detected likely due to low clonal representation in the biopsy.

Next, we aimed to demonstrate the experimental model (PDOX and derived cell lines) generated in the study faithfully represented the clinical sample at PD. To this end we performed computational reconstruction of the tumor clone composition towards the longitudinal samples. By exploiting driver mutations and cognate copy number changes (see Methods), we found that a dominant clone expanded during sotorasib treatment, with the majority of progressing tumor cells harboring *KRAS*$^{G12C}$ and *KEAP1*$^{G476W}$ mutations. This clone further evolved during treatment with the clonal acquisition of *TGFBR2*$^{C421Y}$ and the subclonal heterozygous loss of *KEAP1* (Fig. 2E, F). These results suggest a monoclonal evolution of the tumor that was conserved during the PDOX generation and the subsequent cell line generation, thereby validating our experimental approach as a bona fide model of clinical resistance to sotorasib.

### Validation of acquired genetic alterations as putative mediators of drug resistance

The two PDOX-derived cell lines showed resistance to increasing concentrations of sotorasib in vitro when compared to a panel of *KRAS*$^{G12C}$ control cell lines, thereby indicating that the resistant phenotype was maintained during the orthotopic procedure and the derivation of the cellular models (Fig. 3A).

We then used the PDOX-derived cell lines to validate the candidate molecular mediators of the drug-resistant phenotype. Among the genomic alterations identified in the PD biopsy (Table 1 and Fig. 2B, C) we decided to first focus on *TGFBR2* due to its previously described tumor suppressive function in LUAD[16]. The *C421Y* homozygote alteration identified in the sotorasib-resistant biopsy has not been previously reported.

In vitro characterization suggested an inactivating nature of this substitution as illustrated by the absence of TGFBR-downstream signaling activation upon TGFβ treatment of the PDOX cells when compared to a panel of control LUAD *KRAS*$^{G12C}$ cell lines harboring wild-type

https://doi.org/10.1038/s41467-024-51828-2

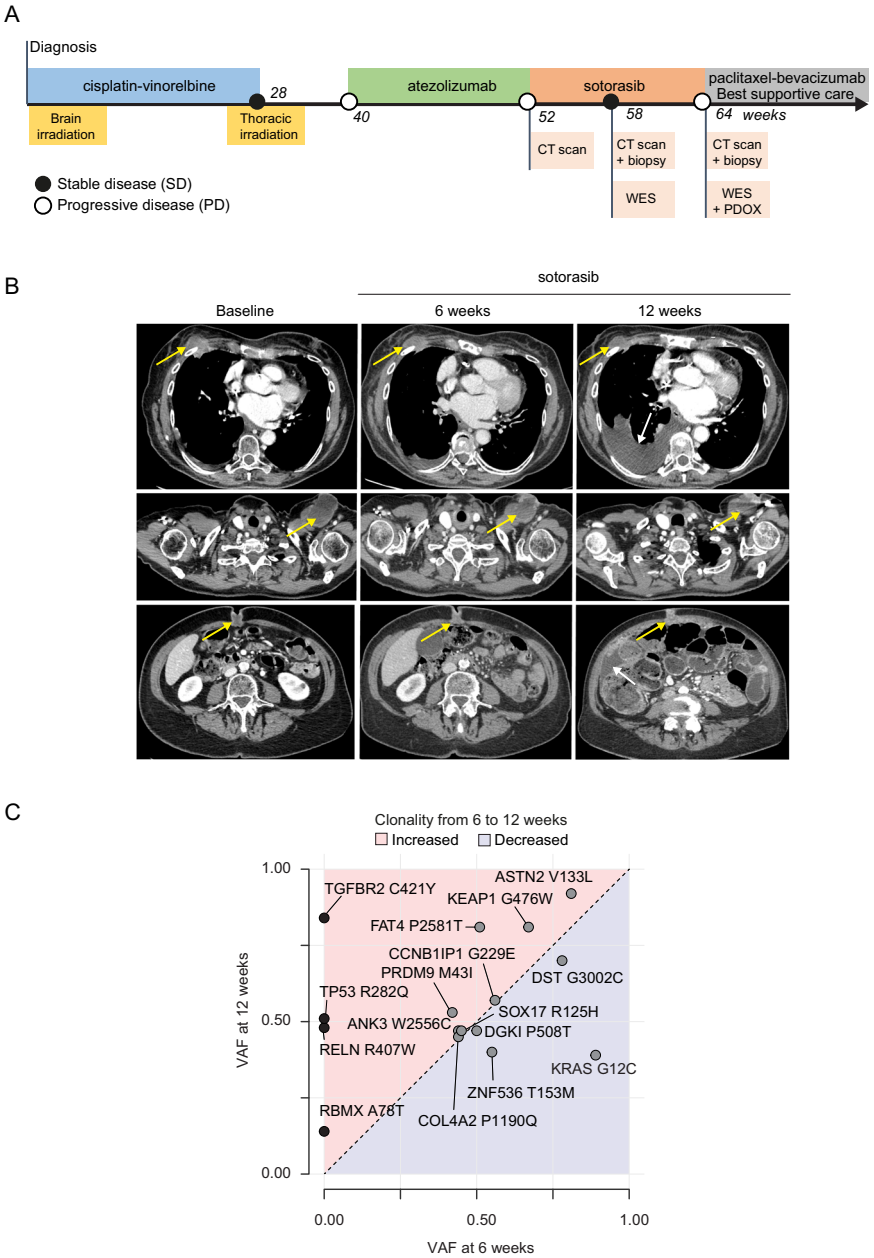


**Fig. 1 | Characterization of LUAD disease progression upon sotorasib (AMG-510) treatment. A** Timeline of the patient clinical record. **B** Computed tomography (CT scan) images showing the evolution of the patient lesions along the sotorasib treatment, including baseline (left), 6 weeks (stable disease, SD, center) and 12 weeks (progressive disease, PD, right). The sequential scans demonstrate an initial stable disease on target lesions: Fourth right rib (top), left pectoral lesion (center), and umbilical lesion (bottom). The latter progressed with right pleural effusion and ascites appearance (white arrows), while the remaining target lesions persisted as stable disease (yellow arrows). **C** Scatter plot (**D**) describing the acquired mutations and their allelic frequencies shared across biopsies on treatment (SD, 6 weeks) and at progression (PD, 12 weeks).

*TGFBR2*. Furthermore, the functionality of the pathway in PDOX cells was restored upon exogenous expression of wild-type *TGFBR2* (Fig. 3B). However, the restoration of an active TGFβ pathway failed to sensitize the PDOX cells to sotorasib, as shown by the absence of additive effect with ZIP synergy score close to zero and a negligible effect in cell proliferation (Fig. 3C–E). Interestingly, the introduction of the C421Y mutant form in H358 cells resulted in pathway inactivation. This is probably due to the putative dominant negative effect of the overexpressed exogenous mutant, further reinforcing the inactivating impact of this substitution (Suppl. Fig. 3A–C). Importantly, the introduction of exogenous $TGFBR2^{C421Y}$ failed to modify the sensitivity to sotorasib despite the dominant negative effect exerted by this mutant on TGFBR-downstream signaling (Suppl. Fig. 3D). Altogether, these results indicated that $TGFBR2^{C421Y}$ was unlikely to be the main driver of the sotorasib-resistant tumor-autonomous phenotype in PDOX cells, at least upon in vitro evaluation.

Next, we evaluated the potential implication of the $KEAP1^{G476W}$ substitution that was enriched in the tumor biopsy performed at disease progression with increased allelic frequency between biopsies (Table 1 and Fig. 2B, C). *KEAP1* mutations have been recurrently associated with drug resistance in LUAD and other cancers[17]. Mutations affecting this residue, including the G476W substitution, have been previously detected in patients with *KRAS*-mutant LUAD[18]. The G476 residue is positioned within a 3D-clustered mutation hotspot[19] suggesting a deleterious effect. To investigate its mechanistic relevance, we generated inducible cell lines to compare the effect of wild-type

**Table 1 | Acquired mutations identified upon progression to sotorasib**

| | 6 weeks | 12 weeks |
|---|---|---|
| ANK3 W2556C | 0.44 | 0.47 |
| ASTN2 V133L | 0.81 | 0.92 |
| CCNB1IP 1 G229E | 0.56 | 0.57 |
| COL4A2 P1190Q | 0.44 | 0.45 |
| DGKI P508T | 0.50 | 0.47 |
| DST G3002C | 0.78 | 0.70 |
| FAT4 P2581T | 0.51 | 0.81 |
| KEAP1 G476W | 0.67 | 0.81 |
| KRAS G12C | 0.89 | 0.39 |
| PRDM9 M43I | 0.42 | 0.53 |
| SOX17 R125H | 0.45 | 0.47 |
| ZNF536 T153M | 0.55 | 0.40 |
| RBMX A78T | - | 0.14 |
| RELN R407W | - | 0.48 |
| TGFBR2 C421Y | - | 0.84 |
| TP53 R282Q | - | 0.51 |

Summary table describing the acquired mutations and their allelic frequencies shared across biopsies on treatment (SD, 6 weeks) and at progression (PD, 12 weeks).

and G476W forms of *KEAP1* on the sensitivity to sotorasib in an isogenic background. This approach demonstrated lower protein expression of the G476W mutant when normalized to the respective mRNA levels suggesting that this mutation results in decreased protein stability (Fig. 3F and Suppl. Fig. 3E). Nevertheless, induction of wild-type or G476W *KEAP1* expression did not impact cell proliferation nor response to sotorasib in vitro (Fig. 3G, H and Suppl. Fig. 3F). Altogether these results suggest that the potential phenotypic consequences brought about by the $KEAP1^{G476W}$ substitution are, similarly to $TGFBR2^{C421Y}$, unlikely to be the main mediators of resistance to sotorasib at least when evaluated in vitro. Nevertheless, we cannot exclude that both TGFBR2 and KEAP1 may play non-cancer autonomous roles in the acquisition of the sotorasib-resistance phenotype not detectable upon in vitro evaluation.

### Adaptive mechanisms potentially contributing to sotorasib resistance in patients

Although we cannot exclude that other genetic alterations identified at disease progression (Table 1 and Fig. 2B), either alone or concomitantly, could be involved in the resistant phenotype, we next considered whether, as previously reported in vitro[11,12], adaptive mechanisms might play a significant role also in patients. Therefore, we screened a cohort of 92 patients with NSCLC treated with KRAS inhibitors at Dana-Farber Cancer Institute (DFCI), and we identified 28 patients with paired archived pre- and post-KRAS inhibitor samples. Interestingly, based on clinically targeted exome sequencing, 10 out of 28 of these patients developed resistance to KRAS inhibitors in the absence of previously described acquired genomic alterations associated with drug resistance. Following quality control filtering, four patients with pre- and post-KRAS inhibitors tumor biopsies had enough leftover material for correlative analysis. Of these, 75% were males, 75% had a history of tobacco use, 75% received sotorasib, and 25% received adagrasib as KRAS inhibitor (Suppl. Table 1). A swimmer plot depicting time on treatment, overall survival, and timing of post-KRASi biopsy is shown in Suppl. Fig. 4. Tumor genomic profiling was performed in 75% of these samples and did not show any clear genomic putative resistance mechanism to KRAS inhibition (Suppl. Table 2). To determine if there were any adaptive resistance mechanisms, we next performed differential gene expression analysis between baseline and KRASi-resistant samples and noted significant upregulation of genes belonging to the RAS signaling pathway (e.g., RACB3, EREG, FGF10, and FGF18) in post-KRASi samples, while there was a downregulation of genes involved in metabolic processes (e.g. CYP2C19, CYP2C8, CYP2C9, CYP3A5, CYP3A7, and CYP7A1) (Fig. 4A). When we performed gene set enrichment analysis, we observed significant upregulation of FGFR signaling, E2F targets, MYC targets, and G2M checkpoint among other pathways in KRASi-resistant samples ($q < 0.05$) (Fig. 4B) suggesting potential changes in the transcriptomic programs of KRASi-resistant tumors. To further characterize changes between paired pre- and post-KRASi samples, we performed single sample gene set enrichment analysis for predefined gene sets involved in RAS signaling as well as in control pathways, including PTEN/AKT and PI3K signaling and noted numerically higher enrichment scores of RAS84 and MAPK signatures[20] in KRASi-resistant samples in three out of four patients (PT1, PT2, and PT4, Fig. 4C). Detailed paired dot plots depicting changes in mRNA expression in 33 genes belonging to the RAS family are shown in Suppl. Fig. 5. Altogether, these observations support the hypothesis that RAS/MAPK signal adaptation may play a crucial role in a subset of KRASi-resistant patients.

### Reversible sotorasib sensitivity in the absence of therapeutic pressure

At this point, we hypothesized that, in the context of adaptive resistance, the elimination of the selective pressure imposed by the drug would phenotypically revert the resistant cells to a sensitive state. To this end, we maintained cultures of the two PDOX cell clones in the absence of sotorasib for 3 weeks before re-evaluating their response to treatment. As shown in Fig. 5A, drug withdrawal partially re-sensitized both clones to sotorasib when compared to the original clones constantly maintained under the selective pressure of the treatment. Sotorasib rechallenge was accompanied by the induction of apoptosis in cells maintained off-drug for 3 weeks (Fig. 5B and Suppl. Fig. 6). Interestingly, PDOX-derived cell lines constantly maintained on sotorasib displayed increased KRAS expression at the protein level (Fig. 5C). This observation suggests that increased KRAS protein levels potentially contribute to the resistant phenotype on top of the additional wild-type *KRAS* allele duplication described above (Fig. 2D). Importantly, this protein increase was also accompanied by elevated levels of active KRAS-GTP, likely applying to both wild-type and mutant $KRAS^{G12C}$ (Fig. 5C). Indeed, the increased *KRAS* expression equally affected the wild-type and G12C alleles as measured by digital droplet PCR, ruling out potential allele-specific expression phenotypes (Fig. 5D and Suppl. Data 4). Using a genome-wide SNP-array, we detected chromosome 12q arm amplification spanning the *KRAS* locus (Fig. 5E and Suppl. Fig. 7), thus confirming the ddPCR results. Remarkably, and in agreement with the adaptive phenotype, the mechanisms controlling KRAS protein levels respond rapidly to the selective pressures imposed by the drug treatment, and the overall KRAS protein levels return to baseline soon after the removal of sotorasib from resistant cell lines (Fig. 5F). On the whole, these results are in agreement with previous in vitro findings[11] and support the idea that adaptive mechanisms leading to augmented KRAS expression and GTP-loading can contribute to resistance to sotorasib.

### The tri-complex inhibitor RMC-4998 overcomes adaptive resistance to sotorasib

Next, we interrogated whether the increase in overall KRAS activity upon exposure to sotorasib would generate a vulnerability when using recently described compounds such as the pan-KRAS(OFF) inhibitor BI-2865 targeting both $KRAS^{G12C}$ and KRAS wild-type[21] or the tri-complex inhibitor RMC-4998 that selectively targets the GTP-bound state of mutant $KRAS^{G12C}$[14,22]. To this end, sotorasib-resistant PDOX cells were exposed to increasing concentrations of BI-2865 or RMC-4998 (Fig. 6A, B and Suppl. Fig. 8A). In agreement with the hypothesis that increased $KRAS^{G12C}$-GTP might be key in the decreased response to

https://doi.org/10.1038/s41467-024-51828-2

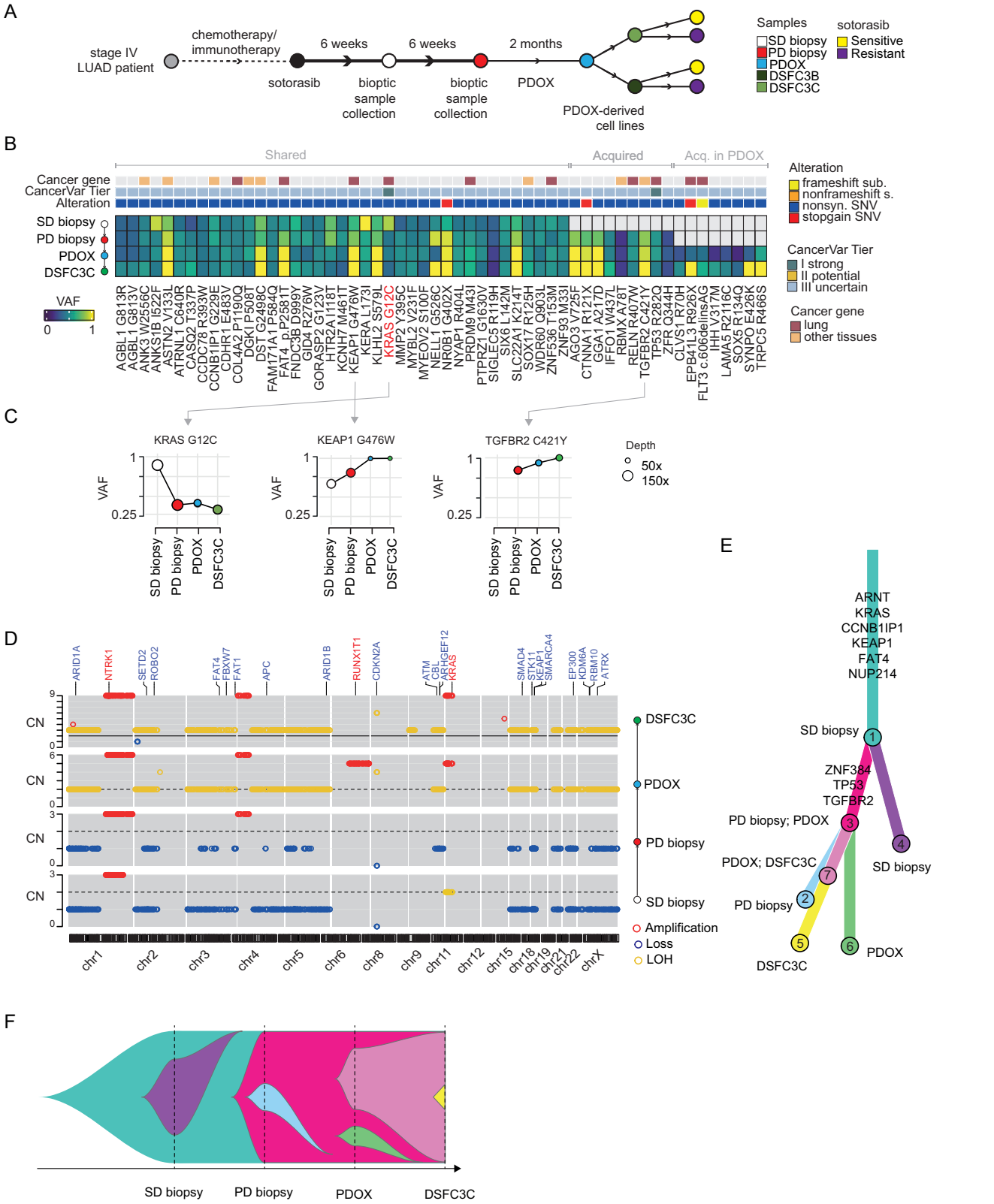


**Fig. 2 | Genomic characterization of longitudinal samples from sotorasib-resistant KRAS$^{G12C}$ LUAD. A** Schematic overview of the longitudinal samples. **B** Heatmap showing the variant allelic frequency (VAF) of somatic mutations present in at least two of the four longitudinal samples. The top annotation heatmap depicts the type of mutation, the cognate damaging effect according to CancerVar (i.e., tier), and the classification of the corresponding gene as cancer genes of lung or other tumors according to the Network of Cancer Genes. **C** Scatter plots show the VAF of selected mutations across the longitudinal samples. **D** View of chromosomal amplifications and losses in the longitudinal samples. Oncogenes (red) and tumor suppressor genes (blue) undergoing amplifications and losses in at least one sample are shown. Loss of heterozygosity (LOH) events are depicted in yellow. **E** Reconstruction of clonal evolution across the longitudinal samples. The evolution of the major clones and minor subclones are shown as colored branches. Tree nodes show samples containing the corresponding clones. **F** Fish plot visualizes clonal evolution across longitudinal samples. Color codes represent clones detected as in (**E**). Source data are provided as a Source Data file.

https://doi.org/10.1038/s41467-024-51828-2

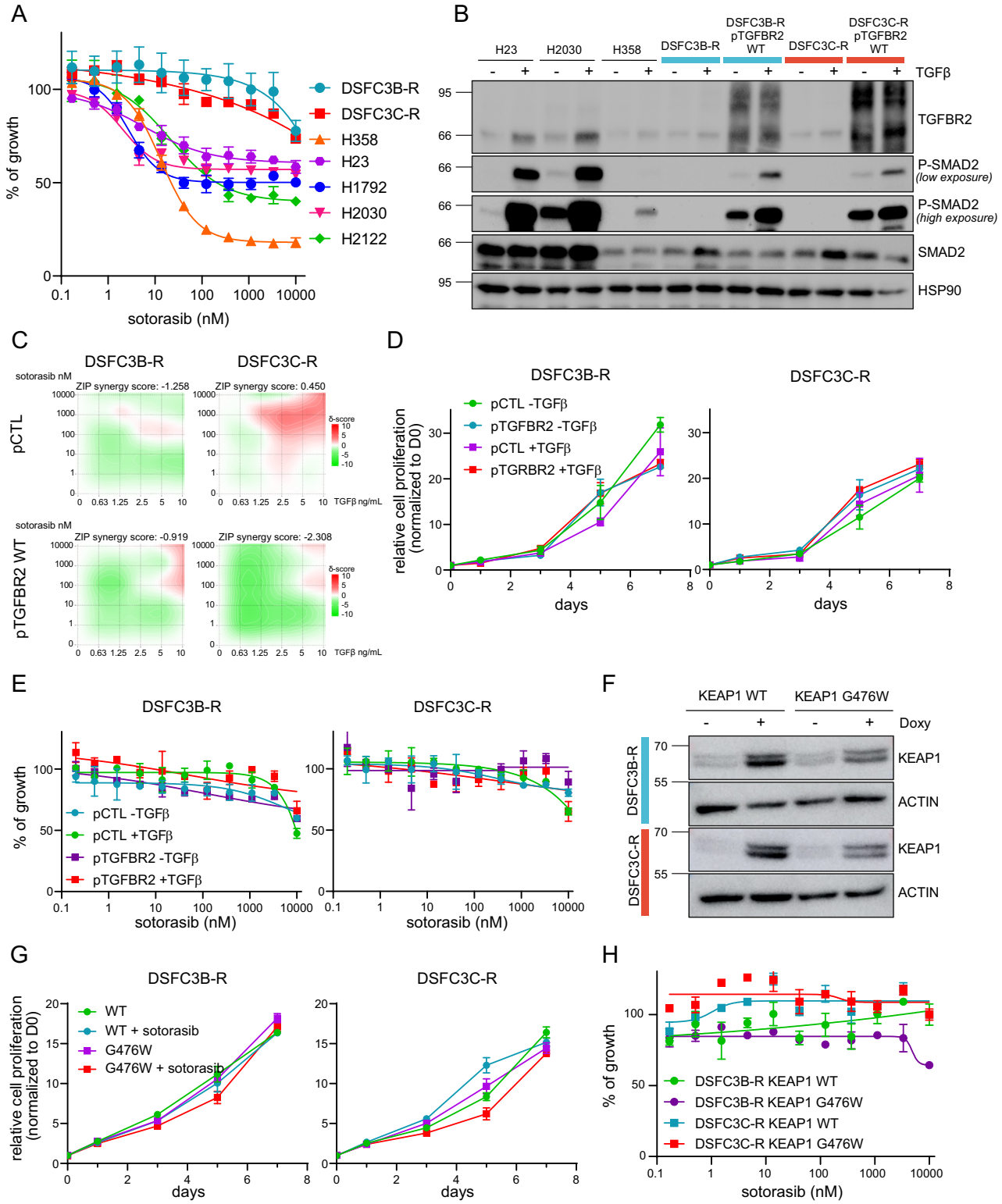


sotorasib, the resistant PDOX cells showed higher sensitivity to RMC-4998. The intermediate sensitivity to BI-2865 suggested that the *KRAS* wild-type allele partly contributed to the phenotype (Fig. 6A, B and Suppl. Fig. 8A). Indeed, to further support the functional relevance of KRAS wild-type in affecting drug sensitivity, we generated an inducible system to tune its expression in PDOX cell lines (Suppl. Fig. 8B). KRAS wild-type expression reduced in a dose-dependent manner the efficacy of sotorasib and RMC-4998, which exclusively target the mutant $KRAS^{G12C}$. On the contrary, BI-2865 efficacy was unaffected by increasing levels of KRAS wild-type, suggesting that in the context of this adaptive phenotype, both wild-type and $KRAS^{G12C}$ should be targeted for optimal therapeutic control (Fig. 6C).

### KRAS(OFF) + KRAS(ON) inhibitors combination in vitro and in vivo

In light of these results, we next evaluated the effect of the KRAS(ON) RMC-4998 inhibition in vivo in the adaptive resistance context. To this end, sotorasib-resistant PDOX cells were implanted in

**Fig. 3 | The acquisition of TGFBR2$^{C421Y}$ and the increased allelic frequency of KEAP1$^{G476W}$ do not drive resistance to sotorasib in PDOX-derived cells. A** Cell viability assay (MTT) was performed with H358, H23, H1792, H2030, H2122, and PDOX-derived (DSFC3B/C-R) cells treated with the indicated concentrations of sotorasib for 72 h. **B** Western blot analysis of TGFβ signaling activation following treatment with TGFβ (5 ng/mL) for 1 h. Extracts were obtained from parental PDOX cells as well as those overexpressing exogenous TGFBR2 WT. KRAS$^{G12C}$ cell lines (H23, H2030, and H358) were used as control. **C** Synergy matrix comparing parental and PDOX cells overexpressing TGFBR2 WT after 72 h in the presence of the indicated concentrations of sotorasib and TGFβ. **D** Proliferation curves of PDOX cells overexpressing exogenous TGFBR2 WT and treated with TGFβ (5 ng/ml) for the indicated time points. **E** Cell viability assay (MTT) was performed with PDOX cells overexpressing exogenous TGFBR2 WT and treated with the indicated concentrations of sotorasib in the presence or absence of TGFβ (5 ng/ml) for 72 h. **F** Western blot analysis of KEAP1 expression in PDOX cells infected with the indicated inducible constructs (KEAP1 WT or G476W) and treated with doxycycline 1 mg/ml for 7 days. **G** Proliferation curves of PDOX cells infected with the inducible KEAP1 WT or G476W construct and treated with doxycycline (1 mg/ml) in the presence or absence of sotorasib (1 μM) for the indicated time points. **H** Cell viability assay (MTT) performed with PDOX cells infected with the inducible KEAP1 WT or G476W construct and treated with the indicated concentrations of sotorasib in presence of doxycycline (1 mg/ml) for 72 h. All data were presented as mean ± SEM from three independent experiments. Representative western blots of two independently performed experiments are shown. Source data are provided as a Source Data file.

immunocompromised mice and randomized to perform treatments with minimal fully efficacious sotorasib dosing according to published data[23]. In agreement with the in vitro data and the patient's medical history, grafted PDOX-resistant cells remained treatment-insensitive and showed a growth rate indistinguishable from that of vehicle-treated controls. Interestingly, if the grafted PDOX tumors were maintained off-treatment, they regained partial sensitivity to sotorasib upon re-challenging. Remarkably, there was a significant inhibition of tumor growth upon daily, oral administration of RMC-4998 when compared to cohorts receiving sotorasib (Fig. 7A). This reduction in tumor growth was accompanied by a decrease in cell proliferation and KRAS downstream signaling as measured by immunostaining detection of phosphorylated histone H3 and ERK1/2 respectively (Fig. 7B). Furthermore, the extent of tumor KRAS$^{G12C}$ target engagement, as evidenced by the shift in RAS mobility caused by covalent binding of the respective inhibitors, was increased in tumors from RMC-4998 treated mice when compared to sotorasib treated mice, likely due to higher KRAS-GTP levels. Likewise, RMC-4998 treatment increased the levels of the pro-apoptotic protein BIM (Fig. 7C). These results suggest that enhanced target engagement and elevated cell death could mediate the improved antitumor activity of RMC-4998.

We next asked whether combinations of RMC-4998 or BI-2865 with sotorasib could improve the therapeutic outcome in the resistant setting. We observed superior efficacy of sotorasib+RMC-4998 compared to sotorasib + BI-2865 in resistant PDOX cells (Fig. 8A). Furthermore, we tested combinations of RMC-4998 with BI-2865, BI-3406, trametinib, and tipifarnib, showing variable degrees of synergistic efficacy compared to single agents alone (Suppl. Fig. 9). Considering that combination treatments with sotorasib could be a feasible strategy to be implemented in the clinical setting of adaptive resistance to sotorasib, we further characterized the sotorasib + RMC-4998 and sotorasib + BI-2865 combinations. Adding RMC-4998 to sotorasib significantly reduced cell proliferation and decreased downstream signaling compared to sotorasib + BI-2865 (Fig. 8B, C and Suppl. Fig. 10A, B). These results are in agreement with the hypothesis that combining RAS(OFF) and RAS(ON) inhibitors in an adaptive resistance context is superior to combining RAS(OFF) inhibitors. Remarkably, we also observed enhanced therapeutic efficacy of the combination treatment sotorasib + RMC-4998 compared to either single agent treatment in vivo in PDOX-resistant xenografts (Fig. 8D, E and Suppl. Fig. 10C).

In sum, these preclinical data suggest that the tri-complex KRAS$^{G12C}$(ON) selective covalent inhibitor RMC-4998 targeting KRAS$^{G12C}$-GTP may offer an alternative therapeutic strategy for the treatment of disease relapse following adaptive resistance to KRAS$^{G12C}$(OFF) covalent inhibitors.

## Discussion

The recent advent of compounds allowing direct inhibition of the *KRAS$^{G12C}$* oncogene such as adagrasib and sotorasib has initiated a new era in the clinical management of various KRAS-driven solid tumors including LUAD. However, despite high initial efficacy, there is a relatively short progression-free survival due to resistance that develops in virtually all patients. In this scenario, novel therapeutic strategies are therefore urgently needed. Multiple mechanisms of resistance have been described in the clinic upon treatment with direct KRAS inhibitors. The molecular basis driving disease progression has been clarified in a subset of cases and includes *cis* mutations on the *KRAS$^{G12C}$* allele affecting the drug-binding pocket, *KRAS* amplification, as well as *MAPK/PI3K* mutations[10,24,25]. The heterogeneity, as well as the presence of multiple subclonal events of such acquired mechanisms, poses difficulties in overcoming resistance to KRAS$^{G12C}$ covalent inhibitors[26]. Yet, the genetic basis underlying disease relapse has not yet been clarified in a significant fraction of resistant tumors.

Preclinical studies had anticipated adaptation and reactivation of RAS-ERK signaling in the form of increased KRAS$^{G12C}$-GTP loading as an additional resistance mechanism[11,12,27]. Here, we provide in vivo evidence in support of KRAS$^{G12C}$ reactivation as a mediator of resistance to sotorasib in patients. A resistant *KRAS$^{G12C}$* LUAD biopsied upon disease progression on sotorasib did not present any of the previously identified mutations which mediate drug resistance by directly affecting either RAS, upstream receptors, or downstream mediators[10,24,27]. We describe the administration of sotorasib selected for the acquisition of an extra copy of the *KRAS* wild-type allele across the resistance cells (Figs. 2, 5). Our interpretation is that fitness advantage on treatment with KRAS(OFF) inhibitors could, in part, be driven by the wild-type *KRAS* allele[13], as previously demonstrated with *KRAS*-LOH (Loss Of Heterozygosity) tumor cells being more sensitive to MEK inhibition[28,29].

We provide experimental evidence addressing the mechanistic implication of two putative variants of *KEAP1* and *TGFBR2* showing higher mutation allele frequency upon sotorasib resistance compared to baseline. Although we exclude the participation of *KEAP1* and *TGFBR2* alterations as main drivers of tumor-autonomous drug resistance, we cannot rule out that in vivo, mechanisms implicating the tumor microenvironment may be dependent on these mutations. A similar rationale could apply to other alterations that were not functionally validated in the current study. Of note, TP53 alterations were excluded for validation as they have recently been shown to have no impact on primary resistance to direct covalent G12C inhibitors in patients with NSCLC[30].

Therefore, we alternatively considered signal adaptation as a potential cause of disease progression. Our results in the index patient indeed suggest that this is a likely scenario, in spite of the fact that the SD biopsy was taken 6 weeks on sotorasib treatment, probably missing the maximal molecular response to the drug and therefore attenuating the magnitude of changes implicated in this adaptation. This hypothesis was further supported by whole transcriptome sequencing on a series of paired pre- and post-KRASi resistance patient samples lacking any clear genomic putative resistance mechanism. We identified transcriptomic correlates of resistance to KRAS inhibitors (Fig. 4), such as upregulation of MAPK and RAS84 signatures[20]. There are limitations that should be acknowledged relative to whole transcriptome analysis

https://doi.org/10.1038/s41467-024-51828-2

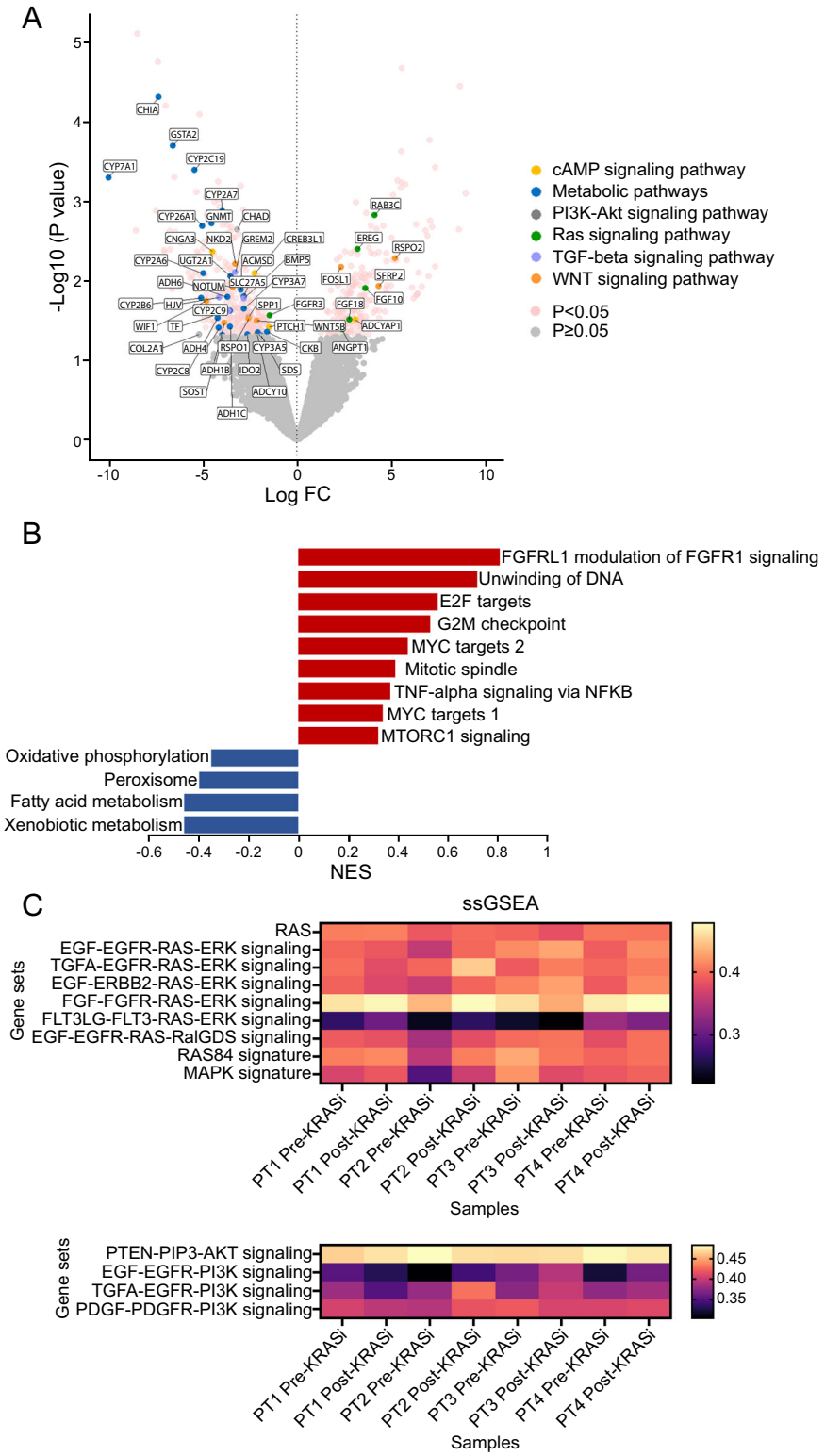


**Fig. 4 | MAPK adaptive activation in patients resistant to KRAS inhibitors.** **A** Volcano plot showing differentially expressed genes in pre- versus post-treatment samples in patients who developed resistance to KRAS inhibitors. Genes of interest are color-coded by pathway according to the Molecular Signatures Database (MSigDB) collections. Differential expression across sample groups was analyzed using the R package edgeR. The threshold for calling a gene as differentially expressed was at least a twofold change (log2FC ≥1 or log2FC ≥−1) with an FDR <0.05. **B** Gene set enrichment analysis showing pathways that are significantly ($Q < 0.05$) up and downregulated in post versus pre-treatment samples. NES normalized enrichment score. **C** Single sample gene set enrichment analysis (ssGSEA) showing enrichment scores of selected pathways involved in the RAS/ERK (upper) and in PI3K/AKT (lower) pathways in paired samples from patients with pre and post-KRAS inhibition tumor samples. Source data are provided as a Source Data file.

https://doi.org/10.1038/s41467-024-51828-2

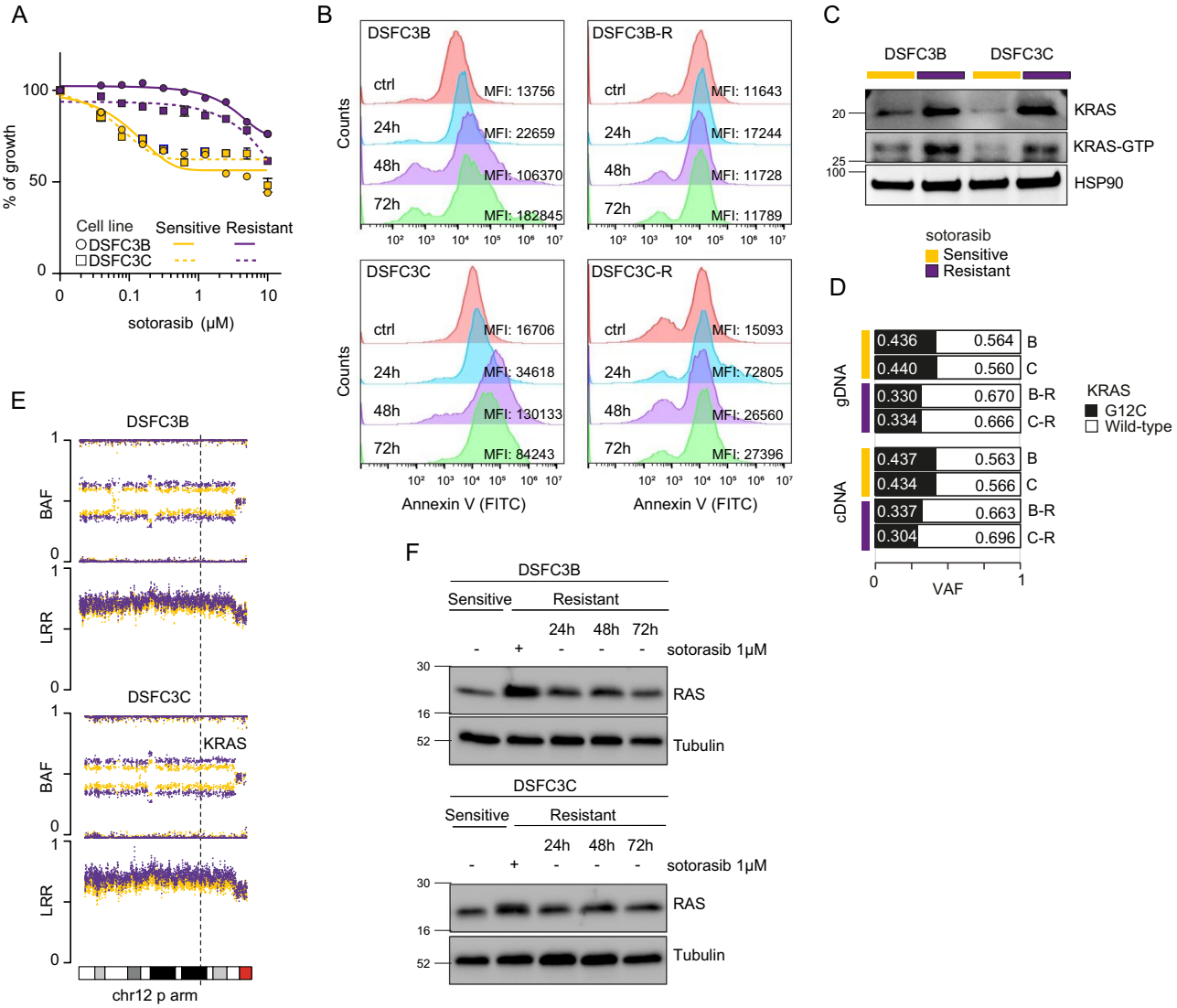


**Fig. 5 | Sotorasib resistance is characterized by increased expression and activation of KRAS. A** Cell viability assay (CellTiter-Glo) comparing PDOX-derived cell lines permanently maintained in 1 μM sotorasib (DSFC3B/C-R) *versus* those subjected to a 3-week drug withdrawal period (DSFC3B/C). Both cell lines were treated with the indicated concentrations of sotorasib for 72 h. Data were presented as mean ± SEM from three independent experiments. **B** Apoptosis of sotorasib sensitive (DSFC3B/C) and resistant (DSFC3B/C-R) PDOX-derived cell lines cells was analyzed by annexin-V staining and FACS analysis following treatment with 10 μM sotorasib for 24, 48, and 72 h. Data were shown as a representative experiment from three independent experiments. **C** Western blot analyses comparing both KRAS and KRAS-GTP levels in PDOX-derived cells maintained in 1 μM sotorasib (DSFC3B/C-R) and following a 3-week drug withdrawal period (DSFC3B/C). Representative western blots of two independently performed experiments are shown. **D** Bar plots show VAF of *KRAS* G12C in PDOX-derived cell lines permanently maintained in 1 μM sotorasib (DSFC3B/C-R) versus those subjected to a 3-week drug withdrawal period (DSFC3B/C) quantified by ddPCR at the RNA (cDNA) level. **E** Scatter plots depict the B-allele frequency (BAF, i.e., the fraction of the signal coming from the allele labeled as **B**) and the Log R Ratio (LRR, i.e., the total intensity of signal) measured for SNPs on the p-arm of chromosome 12 by the OncoScan SNP-array on sotorasib sensitive (DSFC3B/C) and resistant (DSFC3B/C-R) PDOX-derived cell lines. **F** Western blot analysis of RAS expression in DSFC3B/C-R cells after a drug (sotorasib 1 μM) withdrawal period of 24, 48, or 72 h. Representative western blots of two independently performed experiments are shown. Source data are provided as a Source Data file.

performed in patient samples, including the small sample size, the heterogeneity of treatment received prior to KRAS inhibition, and different genomic profiles of these human cancers, which may have impacted these analysis and warrant caution in the interpretation of these results. Nevertheless, these findings suggest the presence of increased active KRAS-GTP at the onset of adaptive resistance. Previously, several studies have associated the elevated KRAS-GTP pool with an attenuated response to KRAS(OFF) compounds. Certain amino acid substitutions such as A59G or Q61L that effectively cancel GTP hydrolysis diminish the response to $KRAS^{G12C}$ inhibitors when introduced as in *cis* mutations[31]. Similarly, SOS1 inhibition enhances the potency of inactive-state selective drugs[32]. Also, the combination of RTK or SHP2 inhibitors decreased KRAS-GTP loading and enhanced both the target engagement and the antitumor activity of RAS(OFF) covalent inhibitors in vivo[33]. In good agreement, our sotorasib-resistant PDOX cells displayed an overall increase in both wild-type and mutant KRAS expression as well as in the active GTP-bound fraction, likely affecting both wild-type and mutant KRAS forms. Interestingly, the mechanism implicated in this cellular adaptation emerges rapidly to the selective pressure imposed by sotorasib treatment as the resistant cultures return to a basal state soon after drug withdrawal in vitro (Fig. 5). Understanding the precise dynamics regulating these fluctuations could provide further insights for therapeutic intervention.

Yet, the sotorasib-resistant PDOX cells remain sensitive to $KRAS^{G12C}$(ON) inhibition by RMC-4998, suggesting that resistance is

https://doi.org/10.1038/s41467-024-51828-2

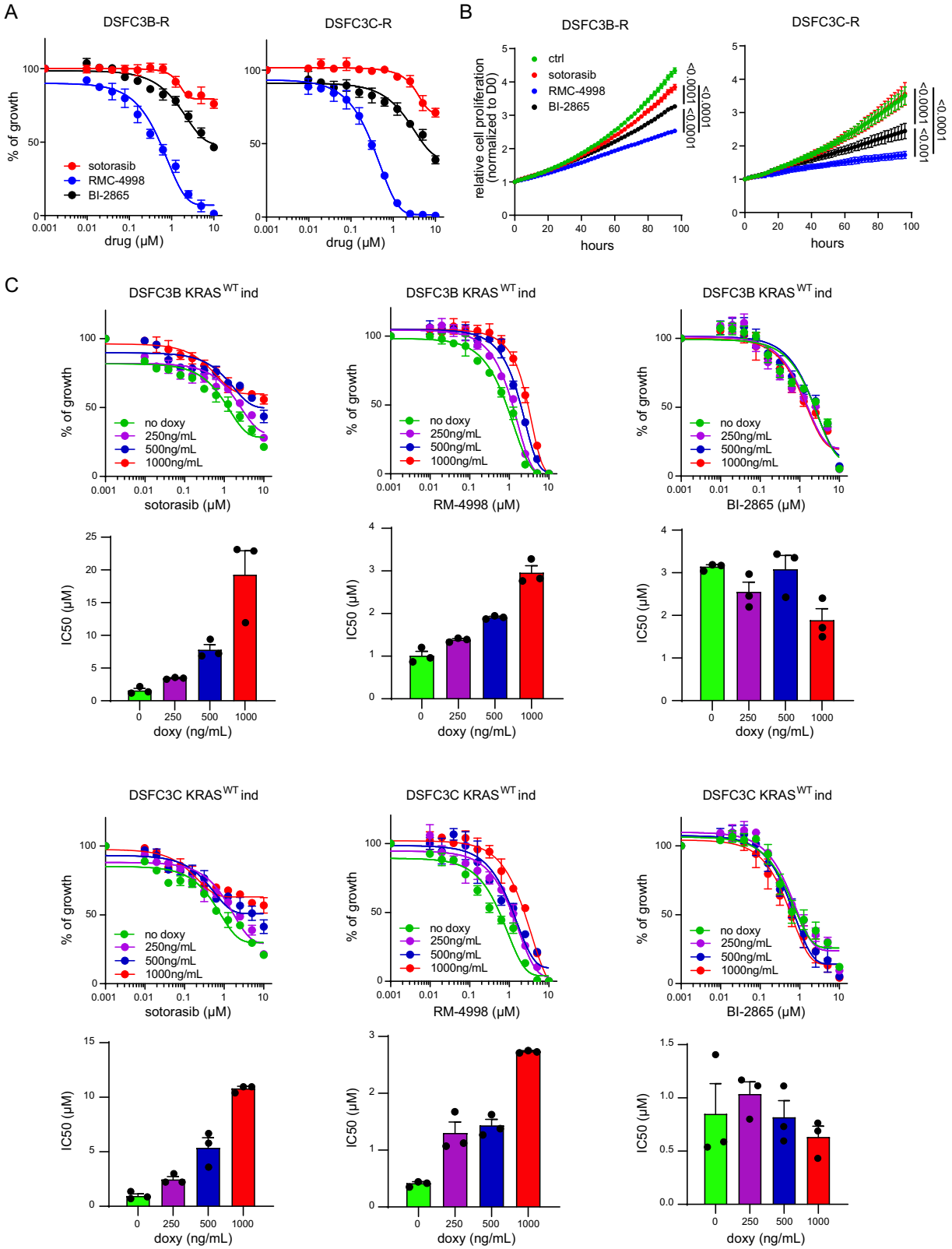


**Fig. 6 | RMC-4998 and BI-2865 exert differential efficacy in sotorasib-resistant PDOX cells in a wild-type KRAS-dependent manner. A**, **B** Cell viability assay (CellTiter-Glo) and Incucyte proliferation assays performed with PDOX-derived (DSFC3B/C-R) cells treated with 1 μM sotorasib, BI-2865 and RMC-4998 for 96 h. Data were presented as mean ± SD from three independent experiments and were analyzed using two-way ANOVA followed by Tukey's multiple comparisons post-test. **C** Cell viability assay (CellTiter-Glo) of PDOX-derived cells infected with wild-type KRAS inducible constructs and treated with increasing doses of doxycycline (up to 1 mg/ml) together with sotorasib, BI-2865 and RMC-4998 for 72 h. Data were presented as mean ± SEM from three independent experiments. Source data are provided as a Source Data file.

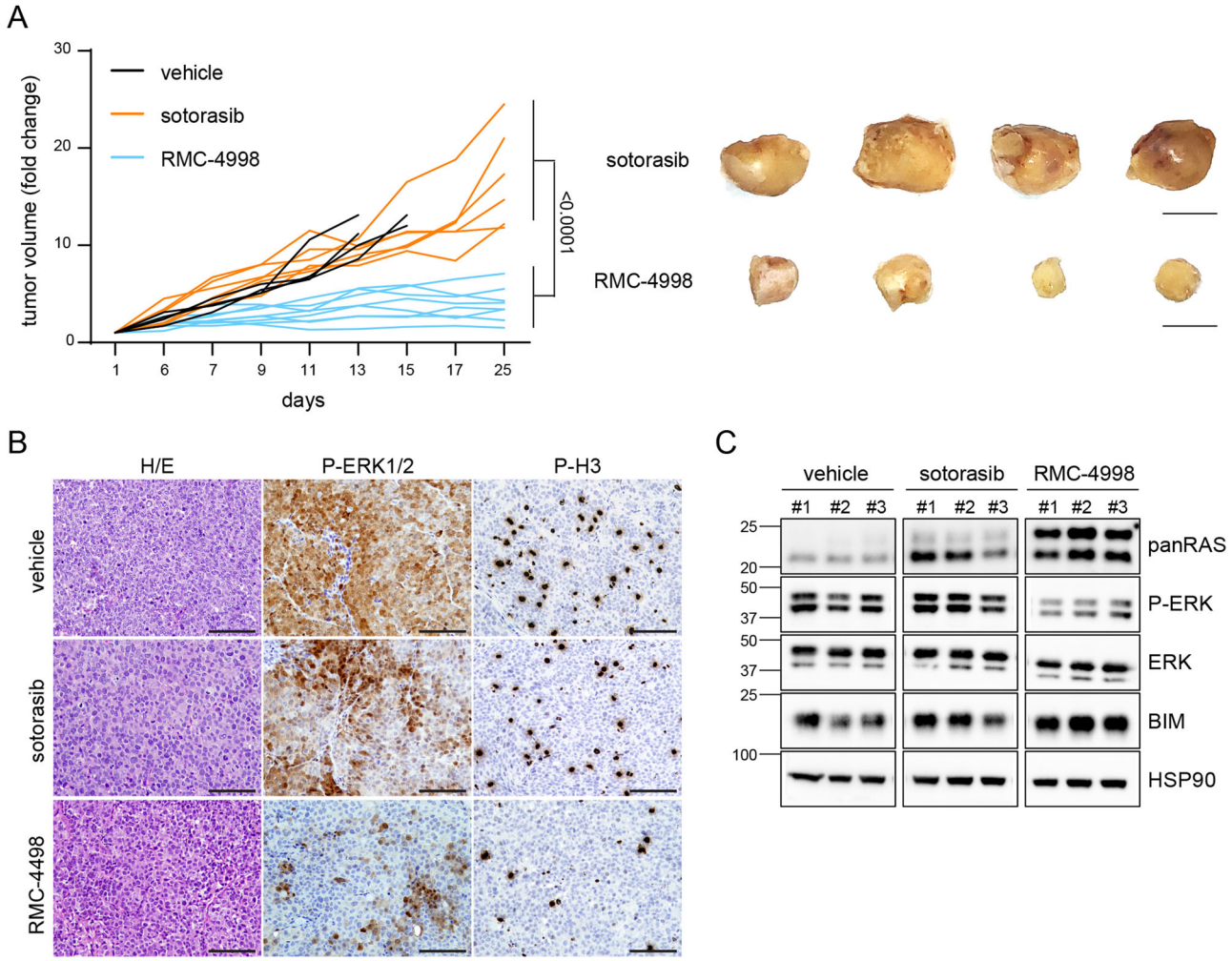


**Fig. 7 | Sotorasib-resistant PDOX cells are sensitive to KRAS(ON) inhibitors in vivo. A** Tumor growth (left) of sotorasib-resistant DSFC3C-R cells following subcutaneous implantation in mice (≥3) and subjected to the indicated treatments (30 and 50 mg/kg qd for sotorasib and RMC-4998 respectively). Each line indicates the volume fold change variation compared to the baseline of each individual tumor. Data were analyzed using one-way ANOVA followed by Tukey's multiple comparisons post-test on the last time point. Representative tumor images at the end of the experiment are also shown (right, scale bar 1 cm). **B** Representative tumor sections following hematoxylin/eosin staining as well as immunostaining with the indicated antibodies. Scale bar 100 µm. **C** Western blot analysis of independent tumor extracts at the end of the experiment shown in (**A**). Low mobility KRAS bands are caused by covalent drug binding. Source data are provided as a Source Data file.

mediated at least in part by increased $KRAS^{G12C}$ GTP-loading. RMC-4998 is selective towards $KRAS^{G12C}$[14], therefore co-targeting both mutant and wild-type active RAS could represent a therapeutic opportunity. The pan-KRAS(OFF) inhibitor BI-2865 targeting both $KRAS^{G12C}$ and KRAS wild-type displayed intermediate efficacy in our models of adaptive resistance, likely due to the major contribution of GTP-bound KRAS. The therapeutic efficacy of $RAS^{MULTI}$(ON) inhibitors such as RMC-6236 (NCT05379985) is currently under clinical assessment and could provide superior activity in this context[34–36].

Our results indicate that inhibitors that target the active state of KRAS, such as the $KRAS^{G12C}$ selective covalent inhibitor RMC-4998 overcome some of the adaptive mechanisms that limit the activity of compounds selective for the inactive state (Fig. 6). This therapeutic approach is currently undergoing clinical evaluation in patients carrying tumors that harbor $KRAS^{G12C}$ mutations (RMC-6291, Phase 1/1b NCT05462717). In our study, the preclinical tool compound RMC-4998 significantly reduced the growth of sotorasib-resistant PDOX implants in vivo (Figs. 7, 8). Interestingly, the combination of sotorasib+RMC-4998 exerted superior therapeutic efficacy, suggesting that KRAS(OFF) + KRAS(ON) inhibitors combined treatment could represent a potential strategy for the management of patients with $KRAS^{G12C}$ LUAD (Fig. 8), if concomitant administration is tolerable. Our results show that the enhanced antitumor effect of RMC-4998 was accompanied by higher target engagement, likely due to the increase in $KRAS^{G12C}$-GTP levels in the resistant setting. Alternatively, greater RMC-4998 exposure compared to sotorasib may also account for this enhanced antitumor activity.

In summary, growing evidences indicate that resistance to KRAS inhibitors is heterogeneous[10,24] and that the identification of specific molecular mechanisms (acquired versus adaptive) needs to be taken into account for subsequent treatment indications. Published evidences[14,22], together with the preclinical results described here demonstrate the potential utility of tri-complex $KRAS^{G12C}$ inhibitors that target the active state of $KRAS^{G12C}$ for the treatment of a subset of patients developing adaptive resistance to covalent RAS(OFF) inhibitors.

## Methods

### Ethics statement

The studies involving patients were conducted in accordance with the International Ethical Guidelines for Biomedical Research Involving Human Subjects (CIOMS) and approved by the Institut Bergonié

https://doi.org/10.1038/s41467-024-51828-2

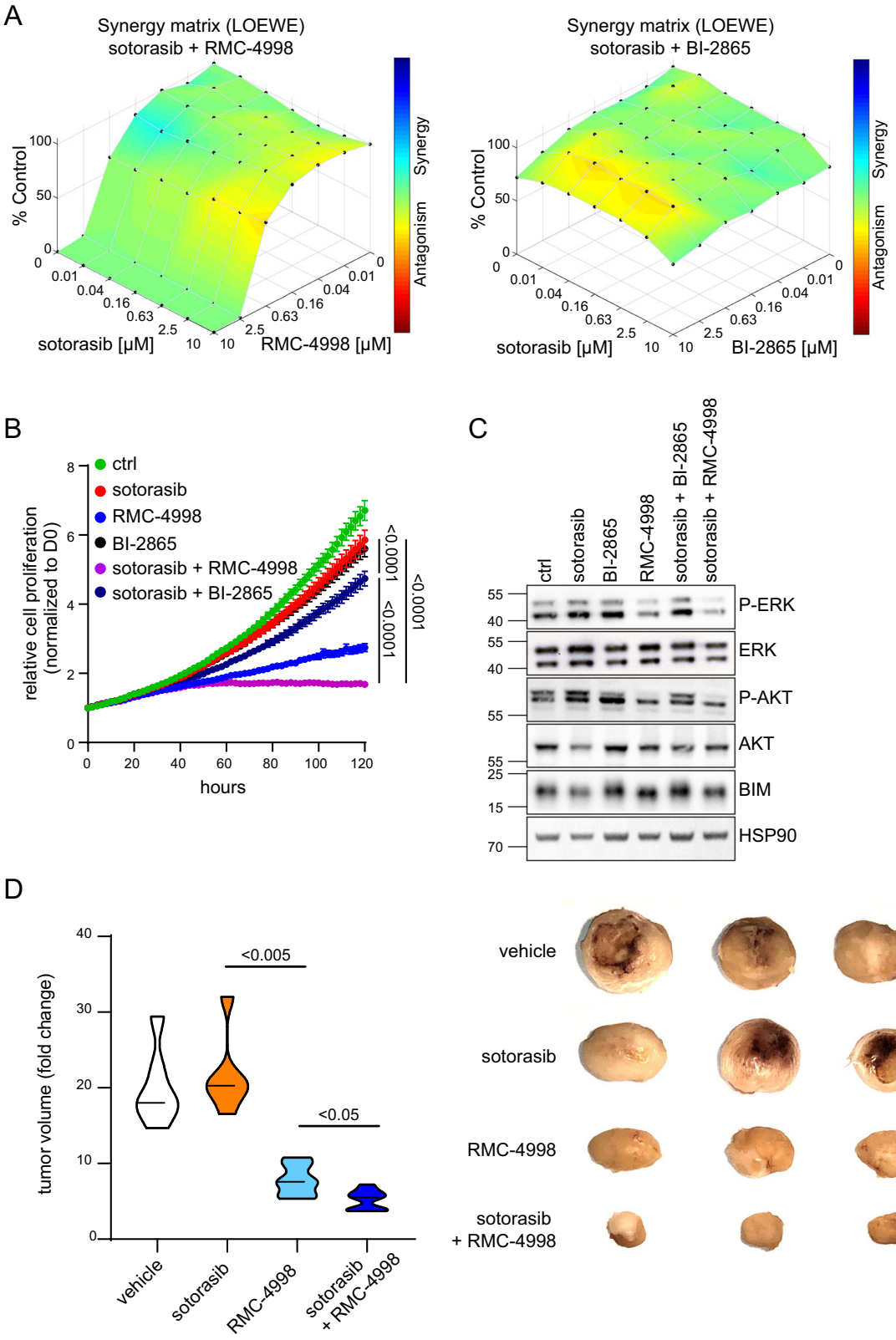


review board. All procedures and animal housing conformed to the regulatory standards and were approved by the Italian Health Minister (authorization n° 1227/2020-PR). Similarly, the animal experimental design involving orthotopic implantation was approved by the IDIBELL animal facility committee (AAALAC Unit1155) and received procedure reference# 9111. All experiments were performed in accordance with the guidelines for Ethical Conduct in the Care and Use of Animals as stated in The International Guiding Principles for Biomedical Research Involving Animals, developed by the Council for International Organizations of Medical Sciences. Patient studies were conducted according to the ethical guidelines of the Declaration of Helsinki. De-identified patient data were used from patients who consented to IRB-approved protocols Dana-Farber/Harvard Cancer Center 02-180, and/or 17-000.

**Fig. 8 | Sotorasib + RMC-4998 combination shows superior efficacy compared to a single agent in vitro and in vivo. A** Synergy matrix in resistant PDOX cells in the presence of the indicated concentrations of sotorasib, BI-2865, or RMC-4998. Data were shown as a representative experiment from six replicates in two independent experiments. **B** Incucyte proliferation assays performed with PDOX-derived (DSFC3C-R) cells treated with 1 μM sotorasib, 0.5 μM BI-2865, and 0.2 μM RMC-4998 as single agents or in combination for 120 h. Data were presented as mean ± SD from three independent experiments and were analyzed using two-way ANOVA followed by Tukey's multiple comparisons post-test. **C** Western Blot analysis of PDOX-derived (DSFC3C-R) cells treated with 1 μM sotorasib, 0.5 μM BI-2865, and 0.2 μM RMC-4998 as single agents or in combination for 24 h. Representative western blots of two independently performed experiments are shown. **D** Violin plot (left) representing tumor volume fold change of sotorasib-resistant DSFC3C-R cells following subcutaneous implantation in mice (≥3) and subjected to the indicated treatments with sotorasib, RMC-4998 (100 mg/kg qd) or the combination for 3 weeks. Representative tumor images at the end of the experiment are also shown (right, scale bar 1 cm). Data were analyzed using one-way ANOVA followed by Tukey's multiple comparisons post-test. Source data are provided as a Source Data file.

### DNA extraction and whole-exome sequencing of patient biopsies

The patient was enrolled in the AMG-510-20170543 phase I/II clinical trial and consented to undergo a biopsy on treatment and at tumor progression. Both frozen specimens were assessed on cryo-sections and tumor cellularity was estimated at this stage. For whole-exome sequencing (WES), DNAs were extracted from frozen biopsy samples and peripheral blood using the QIAamp DNA® Mini kit (Qiagen) following the manufacturer's instructions. WES was performed by IntegraGen SA (Evry, France). Libraries were prepared with the Twist Library Preparation EF kit and captured by the Twist Human Core Exome Enrichment System (Twist Bioscience) and Integragen Custom V2 following the manufacturer's protocol. Captured libraries were sequenced on a NovaSeqTM 6000 sequencing System (Illumina, San Diego, CA, USA) in a 100nt-long paired-end modality.

### Whole transcriptome sequencing

Consecutive slides from patients with G12C-mutant NSCLC who received direct KRAS G12C inhibitors at the DFCI and had consented to IRB-approved correlative protocol DFCI/HCC 02-180 were included. A total of eight FFPE-derived DNase-treated RNA samples extracted at CAMD were submitted for whole transcriptome sequencing. We quantified samples using a fluorescent-based assay (Qubit RNA High Sensitivity assay; Thermo Fisher Scientific) that specifically targets RNA. RNA integrity was assessed using an Agilent RNA 6000 Pico Bioanalyzer kit and found to have a DV200 score (% of RNA at or above 200 nts) of ~50–70%, indicating good quality for FFPE RNA samples. Removal of rRNA was performed using a KAPA RiboErase assay (Roche) according to the manufacturer's protocol. RNA samples were converted to ds-cDNA using a KAPA RNA HyperPrep kit (Roche). Due to the level of RNA degradation, samples were not fragmented but instead denatured at 65 °C for 1 min and then placed on ice. First and second strand synthesis were performed according to manufacturer's recommendations. Following second-strand synthesis, reactions were purified via SPRI-cleanup (KAPA Pure Beads) and then eluted in 53 μl of dH2O. A total of 50 μl of eluate was transferred to new tubes. Samples were converted to Illumina-compatible libraries using a KAPA HyperPrep kit (DNA workflow) and IDT UDI-UMI adapters. The manufacturer's recommendations were followed. Adapters were used at a concentration of 1.5 μM. Post-ligation PCR was conducted for 12 cycles. SPRI-cleaned PCR reactions were eluted in 25 μl of $dH_2O$. Libraries were quantified via Qubit HS dsDNA assay and then assessed with an Agilent High Sensitivity (HS) DNA Bioanalyzer assay. Libraries were pooled by equal volume followed by SPRI-cleanup to remove adapter-dimers then sequenced on an Illumina MiSeq nano flow cell to estimate each library's concentration based on the number of index reads per sample. Library construction is considered successful if the yield is ≥1 nM. All samples were successful. Libraries were normalized using MiSeq-derived concentrations, pooled, SPRI-cleaned one additional time (to remove adapter-dimers and low molecular weight species of ~35 bps) using KAPA Pure Beads, then loaded on 1 NovaSeq SP-200. The run parameters used were 98, 14, 8, and 98. The splice-aware aligner STAR (version 2.4.2a) (https://github.com/alexdobin/STAR) was used to align sequencing reads against the human genome reference hg38. Alignment was followed by QC with Picard Tools (https://broadinstitute.github.io/picard/). The bioinformatics package RSEM (v1.3.1) https://github.com/deweylab/RSEM was used to bin STAR-aligned sequencing reads by genes according to an Ensembl gene feature file for mm9/NCBIM37 release 66.

Expression was given as transcript-length and total-read-normalized read counts (TPM/RPKM). Differential expression across sample groups was analyzed using the R package edgeR (https://bioconductor.org/packages/release/bioc/html/edgeR.html). The thresholds for calling a gene as differentially expressed was at least a twofold change (log2FC ≥1 or log2FC ≤−1) with an FDR <0.05. ssGSEA analysis was conducted to calculate an enrichment score for each pathway of interest for each sample using the GSVA R package. Heatmap was plotted across samples, with color and density indicating the enrichment. The over-representation of the DE genes was investigated using clusterProfile based on KEGG, Gene Ontology, and Reactome database, and $Q$ value <0.05 indicates statistical significance.

### Clinical tumor genomic profiling of FFPE samples

Tumor genomic profiling and somatic variants were performed using our clinically validated OncoPanel platform. Sequence reads were aligned to reference sequence b37 edition from the Human Genome Reference Consortium using bwa (http://biobwa.sourceforge.net/bwa.shtml), and further processed using Picard (version 1.90, http://broadinstitute.github.io/picard/) to remove duplicates and Genome Analysis Toolkit (GATK) to perform localized realignment around indel sites. Single nucleotide variants were called using MuTect v1.1.4, insertions and deletions were called using GATK Indelocator, and variants were annotated using Oncotator. In the DFCI cohort, to filter out potential germline variants, the standard pipeline removed SNPs present at >0.1% in the Exome Variant Server, NHLBI GO Exome Sequencing Project (ESP) (URL: http://evs.gs.washington.edu/EVS/), present in dbSNP, or present in an in-house panel of normals, but rescues those also present in the COSMIC database. Reports and medical records from patients who had their NGS performed at a different institution were manually reviewed.

### Sequence alignment and variant calling

Somatic mutations were identified following our published pipeline[37] as implemented in the HaTSPiL framework[38]. Briefly, sequencing reads from each sample were aligned to the human genome reference (GRCh37/hg19) using Novoalign (http://www.novocraft.com/) with default parameters. At most, three mismatches per read were allowed and PCR duplicates were removed using the Picard Markduplicates tool. Local realignment around small insertion/deletions (InDels) was performed using GATK RealignerTargetCreator and IndelRealigner tools. Single nucleotide variants (SBSs) and InDels were identified using MuTect v.1.1.17[39], Strelka v.1.0.15[40], and Varscan2 v.2.3.6[41] in tumor and normal samples independently. Only variants identified as "KEEP" and "PASS" in MuTect and Strelka, respectively, were considered. SBSs and InDels were retained if (i) had allele frequency ≥5% and (ii) in a genomic position covered by at least ten reads.

### Copy number variant calling and estimation of tumor purity and ploidy

Somatic copy number variants (CNVs) were identified using: (i) sequenza v.3.0.0[42] with parameters window = 5 mb and min.reads.baf = 4, keeping only positions that are covered at least by ten reads, and (ii) EXCAVATOR2[43] with binsize = 20,000 and mode = paired, respectively. To identify amplified and deleted genes, the genomic coordinates of the aberrant regions were intersected with those of 20,297 human protein coding genes of the GENCODE GRCh37 version 28[44]. A gene was considered as modified if ⩾80% of its length was contained in an aberrant region. Tumor ploidy and purity estimates were calculated using sequenza (Suppl. Table 1).

### Identification of putative driver mutations and CNVs

In the tumor samples, mutations were identified as somatic if absent in the normal counterpart. Variant allelic frequencies were corrected by the tumor content reported by Sequenza, as previously described in ref. 37. ANNOVAR[45] was used to identify nonsilent (i.e., nonsynonymous, stopgain, stoploss, frameshift, nonframeshift, and splicing modifications) mutations using RefSeq v.64 (http://www.ncbi.nlm.nih.gov/RefSeq/) as a reference protein dataset. Mutations falling within 2 bp from the splice sites of a gene were considered splicing mutations. Next, a list of cancer genes was retrieved from the Network of Cancer Genes v.7[46] (http://ncg.kcl.ac.uk/). This list was exploited to select 2046 cancer driver genes, respectively. Of these, 203 were lung cancer driver genes. Next, a list of 164 genes with actionable alterations was collected from the "PrecisionTrialDrawer" R package[47] and considered as actionable genes. Finally, a list of eight genes (i.e., *ALK*, *BRAF*, *EGFR*, *KRAS*, *MET*, *ERBB2*, *ARAF*, and *MAP2K1*) with oncogenic mutations that are therapeutically targeted with drugs as reported in the precision Oncology Knowledge Base (OncoKB, https://www.oncokb.org/) data repository was collected. Genes harboring nonsilent mutations were annotated using these three gene lists. Next, CancerVar[48] was used to classify the pathogenicity of somatic variants according to AMP/ASCO/CAP/CGC 2017-2019 guidelines[49]. Mutations classified by CancerVar as "benign" (i.e., Tier IV) were excluded. Retained mutations were considered as putative cancer drivers if (i) annotated by CancerVar as variants of strong or potential clinical significance (i.e., Tier I and II), or (ii) identified by at least two variant callers or in genes annotated as cancer driver and/or actionable.

Similarly, genes were considered undergoing driver CNVs if (i) identified by sequenza and EXCAVATOR2, (ii) with a probability of being a specific copy number state as measured by EXCAVATOR2 greater than 0.75, and (iii) annotated as lung cancer driver and/or actionable.

### Evaluation of clonal evolution

Driver mutations and cognate copy number status were used to infer the clonal population structure of the tumor. In particular, PyClone version 0.13.1[50] was exploited to group driver mutations into clonal clusters and estimate their cellular prevalence. The algorithm was run with efault parameters and tumor purity information estimated as described above. Phylogenetic reconstruction of clonal evolution was performed using the *clonevol* R package v. 0.99.11[51]. In particular, clonal clusters detected by Pyclone were used as input of the *infer.clonal.models* function. Clusters containing less than ten variants were excluded to avoid possible biases in the phylogenetic reconstruction as required by clonevol. Evolutionary tree was built using the *convert.consensus.tree.clone.to.branch* function with the squared root as branch scale. The evolutionary tree was visualized using the *plot.clonal.models* function.

### Cell lines and reagents

H358, H23, H1792, H2030, and H2122 human $KRAS^{G12C}$ lung cancer cells, purchased from American Type Culture Collection (ATCC), were maintained in RPMI medium containing 10% fetal bovine serum (FBS) under standard culture conditions. All cell lines were regularly checked for mycoplasma contamination. Sotorasib (TargetMol, T8684) and recombinant human TGFβ1 (ABclonal, RP00451) were used at the indicated concentrations. RMC-4998 was provided by Revolution Medicines, and details can be found in ref. 14. Modified cell lines are available upon request through MTAs.

### Generation of a patient-derived orthotopic xenograft (PDOX/orthoxenograft) and PDOX-derived cell lines

The establishment of PDOX-derived cell lines was performed as previously described in ref. 15. Briefly, within 24 h following surgical resection, a small tumor biopsy was introduced into the chest cavity of Crl:NU-*Foxn1*$^{nu}$ female mice (Envigo) and anchored to the lung surface with Prolene 7.0 suture. The implanted lung tumor was harvested at a humane endpoint (2 months from implantation), cut into small fragments of 2 to 4 $mm^3$, and serially transplanted into three new animals. The entire in vivo expansion was carried out in the absence of sotorasib. In order to derivate matched cell lines, freshly collected lung tumor tissues coming from orthotopic implants from two independent mice were minced with sterile scalpels and cultured in RMPI medium with sotorasib 1 μM. The established cell lines (DSFC3B/C-R) were maintained in the presence of sotorasib 1 μM for several passages. In parallel, DSFC3B/C cells were cultured in the absence of sotorasib for 3 weeks before re-evaluating their response to treatment.

### SNP-array and CNV detection

DNA was extracted from formalin-fixed paraffin-embedded (FFPE) cell lines using the QIAamp® DSP DNA FFPE Tissue kit (Quiagen) according to the manufacturer's recommendations and quantified using the NanoDrop 2000 (Thermo Scientific) and Qubit (Qubit 3.0 Fluorometer, Life Technologies). SNP-array was performed according to the OncoScan® FFPE SNP-array kit procedure (Affymetrix). Sample preparation, hybridization, and scanning procedures were performed according to the manufacturer's protocol on the Affymetrix GeneChip Scanner 3000 7G system. Raw data were analysed using the EaCoN R package (https://github.com/gustaveroussy/EaCoN) developed at the Gustave Roussy institute following the authors' instructions. In particular, AT and GC channel CEL files were normalized using the *OS.processed* function with default parameters. Then, normalized data were segmented using the *Segment.ff* function and sequenza algorithm as segmenter. Finally, copy number estimation was performed using the *ASCN.ff* function with default parameter.

### Digital droplet PCR validation of $KRAS^{G12C}$

The allelic variant frequency of KRAS G12C at genomic and transcriptomic levels was quantified using digital droplet PCR (ddPCR) as previously published[52]. Briefly, genomic DNA and total RNA were extracted from PDOX-derived sensitive (DSFC3B/C) and resistant (DSFC3B/C-R) cells using DNeasy Blood & Tissue Kits (69504, Qiagen) and TRIzol™ (15596018, Thermo Scientific™) respectively, according to manufacturer's instructions. RNA samples were then subjected to DNAse treatment and purification using RNA Clean & Concentrator-5 (R1014, Zymo Research). One-step reverse transcriptase was performed using Maxima H Minus Reverse Transcriptase (EP0751, Thermo Scientific™), using only Oligo(dT)18 as a primer (SO131, Thermo Scientific). ddPCR was performed using the QX200 Droplet Digital PCR System (1864001, Bio-Rad). Droplets were generated using the QX200 Droplet Generator (1864002, Bio-Rad) in a total volume of 20 μL containing either 10 ng of input gDNA or cDNA corresponding to 1.5 ng of input RNA, 900 nM/250 nM final concentration of KRAS G12C primers/probe, and 10 μL of 2X ddPCR Supermix for Probes (No dUTP) (1863024, Bio-Rad). PCR reactions were executed according to the manufacturer's instructions as follows: enzyme activation at 95 °C for 10 min (1 cycle), denaturation at 94 °C for 30 s followed by annealing/extension at 55 °C for 1 min (40 cycles), enzyme deactivation at 98 °C

for 10 min (1 cycle), and hold at 4 °C. After PCR completion, droplets were processed with the QX200 Droplet Reader (1864003, Bio-Rad) and analyzed using QuantaSoft software (1864011, Bio-Rad). Total events in each sample replicate were quantitated using the mean copy number per µl (Suppl. Data 4). Primers and probes for KRAS G12C available from Bio-Rad were used for genomic DNA mutation assay. Conversely, primers and probes for KRAS G12C mutation assay on cDNA were taken from ref. 53.

### Quantitative PCR (RT-qPCR) analysis

Total cellular RNA was extracted using a Nucleospin RNA Mini kit (Macherey-Nagel) and reverse-transcribed using Transcriptor First Strand cDNA Synthesis kit (Roche), according to manufacturers' instructions. cDNAs were subjected to PCR amplification and quantification. Primer sets included human *KEAP1*-Fwd (5′-CAACTTCGCTGA GCAGATTGGC-3′), human *KEAP1*-Rv (5′-TGATGAGGGTCACCAGTT GGCA−3′), human *18S*-Fwd (5′-GCGGCGGAAAATAGCCTTTG-3′), and human *18S*-Rv (5′-GATCACACGTTCCACCTCATC−3′).

### Tissue processing and immunohistochemistry

Tumor samples derived from mouse implants were fixed in 10% buffered formalin (Sigma), embedded in paraffin, and evaluated by conventional Haematoxylin & Eosin (H&E) staining. Antibodies used for immunostaining included those raised against pERK1/2 (Cell Signaling Technology; 9101), phosphorylated Histone 3 (06-570, Millipore), CK7 (OV-TL 12/30, Agilent-Dako), CK20 (Ks20.8, Agilent-Dako), Napsin A (TMU-Ad02, Biocare Medical), TTF1 (8G7G3/1, Agilent-Dako), p40 (BC28, Gennova), Chromogranin (Agilent-Dako), and Synaptophysin (SY38, Agilent-Dako).

### Plasmids and site-directed mutagenesis

pHAGE-TGFBR2 was a gift from Gordon Mills & Kenneth Scott (Addgene plasmid #116800)[54]. *KEAP1* cDNA isolated from 3xFLAG pcDNA 4 KEAP1 (kind gift of Prof. Susumu Imaoka, Kwansei Gakuin University, Sanda, Japan[55]) and WT KRAS-V5 were cloned in doxycycline-inducible pCW57.1 plasmid (a gift from David Root, Addgene plasmid #41393). All mutations were generated by site-directed mutagenesis using the Q5 site-directed mutagenesis kit (New England BioLabs) according to the manufacturer's instructions. All constructs were re-sequenced to ensure that no undesirable mutation had been introduced.

### Cell viability assays

Cell lines were seeded in 96-well plates at 2–5 × $10^3$ cells/well and treated with a serial dilution of drugs for 72 h. Cell viability was assessed by MTT (Sigma) or by CellTiter-Glo (Promega) assays, as mentioned in figure legends. The synergy between two compounds was assessed using the Zero Interaction Potency (ZIP) method and the open-source SynergyFinder 3.0 software[56,57] or the Combenefit tool, using the Loewe additivity model[58]. For apoptosis assessment by FACS, cells (250,000 cells/well) were plated on six-well plates. The following day, the cells were subjected to treatment protocols with 10 µM sotorasib for the indicated times. Cells were trypsinized and washed with PBS and with an annexin binding buffer. Cell pellets were then suspended in 100 µl annexin binding buffer containing 5 µl of annexin-V Alexa Flour 488 conjugate (Life Technologies) and PI solution at the final concentration of 10 µg/ml, followed by incubation for 15 min in the dark. About 400 µl of annexin binding buffer was added before the samples were analyzed by FACS. Cells were gated according to their SSC/FSC features. Cell doublets were discriminated and excluded from the analysis. PI and Annexin-V positive cells were gated to identify apoptotic cells. Unstained cells were used to set up the gating strategy for FL-1 (Annexin-V) and FL-3 channels (PI). Data were analyzed using the FlowJo software.

### Cell proliferation assays

PDOX-derived cell lines were seeded in 96-well plates at 5 × $10^3$ cells/well and treated with sotorasib (1 µM) and doxycycline (1 mg/ml) for 72 h. Cell proliferation was assessed by CyQUANT (Fisher Scientific) assays.

### Western blot analysis

Protein extracts obtained from cell lysates were separated on SDS–PAGE, transferred to a nitrocellulose membrane, and blotted with the indicated primary antibodies. Antibodies against TGFBR2 (#79424, 1:1000), P-SMAD2 Ser465/467 (#3108, 1:1000), SMAD2 (#5339, 1:1000), P-SMAD3 Ser423/425 (#9520, 1:1000), SMAD3 (#9523, 1:1000), KEAP1 (#8047, 1:1000), PERK1/2 (#9101, 1:1000), ERK (#9102, 1:1000), RAS (#8832, 1:1000), BIM (#2933, 1:1000), HSP90 (#4877, 1:2000), V5-Tag (#13202, 1:1000) were purchased from Cell Signaling Technology. The KRAS clone F234 (sc-30, 1:1000, Santa Cruz Biotechnology) was also used for western blot analysis.

### KRAS activation assay

KRAS activity was determined using the active RAS pull-down and detection kit (#11871, Cell Signaling Technology). Briefly, glutathione S-transferase (GST)–RAF1 RAS-binding domain (RBD) and glutathione agarose resin were mixed together with whole-cell lysates and incubated on a rotator for 1 h at 4 °C, followed by three washes and elution with 2× SDS–PAGE loading buffer. The samples were then analyzed by SDS–PAGE and western blot analysis with a RAS or KRAS-specific antibody.

### Mice experiments

In vivo experiments were conducted on 6- to 8-week-old female NSG mice purchased from Charles River. Tumor cells were injected subcutaneously and bilaterally in the hind flanks of the abdomen (1 × $10^6$ cells/site in 100 µl of PBS). Tumors were palpable and measurable after ~2 weeks. Tumor volume was monitored every other day using a caliper and was calculated by the ellipsoid approximation formula: 3.14 × (length × width$^2$)/6. The maximum allowed tumor size according to the applicable Ethical Guidelines was 2000mm$^3$ and was never exceeded during the experimental observation. Drug treatment was initiated 2 days after the first tumor volume measurement at 30 and 50 mg/kg for sotorasib and RMC-4998, respectively. All drugs were administered by oral gavage and were prepared as follow: sotorasib was formulated in 2% (w/v) HPMC (Hydroxypropyl-methyl cellulose—Sigma H8384/ (v/v) 1% tween 80; RMC-4998 was formulated in 10% (v/v) DMSO/20% (v/v) PEG400/10% (v/v) Solutol (Merck Kolliphor® HS 15, 42966) /60% (v/v) 2% HPMC E-50 (w/v) in 50 mM Sodium Citrate Buffer, pH 4.0 according to the manufacturer instructions. The vehicle for the RMC-4998 compound was used as control. Mice were euthanized and tumors were resected. Half of the tumors were snap-frozen, and the second part was fixed in formalin and embedded in paraffin for further analysis.

### Statistics and reproducibility

All experiments were performed as several independent biological replicates. All results are reported as mean ± SEM (standard error of the mean) or ±SD (standard deviation). Statistical analysis was performed using one-way or two-way ANOVA. A $p$ value less than 0.05 was considered significant; $p$ values are provided within each figure legend, together with the statistical test performed for each experiment. $N$ values are indicated within figure legends and refer to either experimental replicates or animal study groups, whereas technical replicates refer to repeated analysis of the same samples. In animal experiments, no data were excluded from the analyses, the experiments were randomized, and the Investigators were not blinded to allocation during experiments and outcome assessment.

### Reporting summary

Further information on research design is available in the Nature Portfolio Reporting Summary linked to this article.

## Data availability

Sequencing data of SD and PD biopsies, PDOX and PDOX-derived cell lines generated in this study have been deposited in NCBI Sequence Read Archive database under the accession code PRJNA1020204 and are publicly available. Processed OncoScan SNP-array data are provided in the GitHub repository [https://github.com/matteocereda/KRASG12C-LUAD]. The data generated in this study are provided in the Source Data file. All remaining information can be found in the Article, Supplementary, and source Data files. Source data are provided with this paper.

## Code availability

The original code has been deposited on GitHub and is publicly available at https://github.com/matteocereda/KRASG12C-LUAD. Any additional information required to reanalyze the data reported in this paper is available from the lead contact upon request.

## References


1. Martínez-Jiménez, F. et al. A compendium of mutational cancer driver genes. *Nat. Rev. Cancer* **20**, 555–572 (2020).
2. Ostrem, J. M., Peters, U., Sos, M. L., Wells, J. A. & Shokat, K. M. K-Ras(G12C) inhibitors allosterically control GTP affinity and effector interactions. *Nature* **503**, 548–551 (2013).
3. Skoulidis, F. et al. Sotorasib for lung cancers with KRAS p.G12C mutation. *N. Engl. J. Med.* **384**, 2371–2381 (2021).
4. Canon, J. et al. The clinical KRAS(G12C) inhibitor AMG 510 drives anti-tumour immunity. *Nature* **575**, 217–223 (2019).
5. Riely, G. J. et al. 99O_PR KRYSTAL-1: activity and preliminary pharmacodynamic (PD) analysis of adagrasib (MRTX849) in patients (Pts) with advanced non–small cell lung cancer (NSCLC) harboring KRASG12C mutation. *J. Thorac. Oncol.* **16**, S751–S752 (2021).
6. Fell, J. B. et al. Identification of the clinical development candidate MRTX849, a covalent KRASG12C inhibitor for the treatment of cancer. *J. Med. Chem.* **63**, 6679–6693 (2020).
7. Perurena, N., Situ, L. & Cichowski, K. Combinatorial strategies to target RAS-driven cancers. *Nat. Rev. Cancer* **24**, 316–337 (2024).
8. de Langen, A. et al. Sotorasib versus docetaxel for previously treated non-small-cell lung cancer with KRASG12C mutation: a randomised, open-label, phase 3 trial. *Lancet* **401**, 733–746 (2023).
9. Hong, D. S. et al. KRAS-G12C inhibition with sotorasib in advanced solid tumors. *N. Engl. J. Med.* **383**, 1207–1217 (2020).
10. Awad, M. M. et al. Acquired resistance to KRAS G12C inhibition in cancer. *N. Engl. J. Med.* **384**, 2382–2393 (2021).
11. Xue, J. Y. et al. Rapid non-uniform adaptation to conformation-specific KRAS(G12C) inhibition. *Nature* **577**, 421–425 (2020).
12. Ryan, M. B. et al. Vertical pathway inhibition overcomes adaptive feedback resistance to KrasG12C inhibition. *Clin. Cancer Res.* **26**, 1633–1643 (2020).
13. Ivanisevic, T. et al. Increased dosage of wild-type KRAS protein drives KRAS-mutant lung tumorigenesis and drug resistance. Preprint at *bioRxiv* https://doi.org/10.1101/2024.02.27.582346 (2024).
14. Schulze, C. et al. Chemical remodeling of a cellular chaperone to target the active state of mutant KRAS. *Science* **381**, 794–799 (2023).
15. Ambrogio et al. Modeling lung cancer evolution and pre-clinical response by orthotopic mouse allografts. *Cancer Res.* **74**, 5978–5988 (2014).
16. Lo Sardo, F. et al. YAP/TAZ and EZH2 synergize to impair tumor suppressor activity of TGFBR2 in non-small cell lung cancer. *Cancer Lett.* **500**, 51–63 (2021).
17. Hellyer, J. A., Padda, S. K., Diehn, M. & Wakelee, H. A. Clinical implications of KEAP1-NFE2L2 mutations in NSCLC. *J. Thorac. Oncol.* **16**, 395–403 (2021).
18. Cerami, E. et al. The cBio cancer genomics portal: an open platform for exploring multidimensional cancer genomics data. *Cancer Discov.* **2**, 401–404 (2012).
19. Gao, J. et al. 3D clusters of somatic mutations in cancer reveal numerous rare mutations as functional targets. *Genome Med.* **9**, 4 (2017).
20. East, P. et al. RAS oncogenic activity predicts response to chemotherapy and outcome in lung adenocarcinoma. *Nat. Commun.* **13**, 5632 (2022).
21. Kim, D. et al. Pan-KRAS inhibitor disables oncogenic signalling and tumour growth. *Nature* **619**, 160–166 (2023).
22. Tanaka, N. et al. Clinical acquired resistance to krasg12c inhibition through a novel kras switch-ii pocket mutation and polyclonal alterations converging on ras–mapk reactivation. *Cancer Discov.* **11**, 1913–1922 (2021).
23. Lanman, B. A. et al. Discovery of a covalent inhibitor of KRASG12C (AMG 510) for the treatment of solid tumors. *J. Med. Chem.* **63**, 52–65 (2020).
24. Zhao, Y. et al. Diverse alterations associated with resistance to KRAS(G12C) inhibition. *Nature* **599**, 679–683 (2021).
25. Salmón, M. et al. Kras oncogene ablation prevents resistance in advanced lung adenocarcinoma. *J. Clin. Invest.* **133**, e164413 (2023).
26. Tsai, Y. et al. Rapid idiosyncratic mechanisms of clinical resistance to KRAS G12C inhibition. *J. Clin. Invest.* **132**, e155523 (2022).
27. Kim, D., Xue, J. Y. & Lito, P. Targeting KRAS(G12C): from inhibitory mechanism to modulation of antitumor effects in patients. *Cell* **183**, 850–859 (2020).
28. Ambrogio, C. et al. KRAS dimerization impacts MEK inhibitor sensitivity and oncogenic activity of mutant KRAS. *Cell* **172**, 857–868 (2018).
29. Burgess, M. et al. KRAS allelic imbalance enhances fitness and modulates MAP kinase dependence in cancer. *Cell* **168**, 1–13 (2017).
30. Negrao, M. et al. Co-mutations and KRAS G12C inhibitor efficacy in advanced NSCLC. *Cancer Discov.* 13, 1556–1571 (2023).
31. Lito, P., Solomon, M., Li, L.-S., Hansen, R. & Rosen, N. Allele-specific inhibitors inactivate mutant KRAS G12C by a trapping mechanism. *Science* **351**, 604–608 (2016).
32. Hillig, R. C. et al. Discovery of potent SOS1 inhibitors that block RAS activation via disruption of the RAS–SOS1 interaction. *Proc. Natl Acad. Sci. USA* **116**, 2551–2560 (2019).
33. Hallin, J. et al. The KRAS G12C inhibitor, MRTX849, provides insight toward therapeutic susceptibility of KRAS mutant cancers in mouse models and patients. *Cancer Discov.* **10**, 54–71 (2019).
34. Holderfield, M. Concurrent inhibition of oncogenic and wild-type RAS-GTP for cancer therapy. *Nature* **629**, 919–926 (2024).
35. Wasko, U. N. et al. Tumor-selective effects of active RAS inhibition in pancreatic ductal adenocarcinoma. *Nature* **629**, 927–936 (2024).
36. Jingjing, J. et al. Translational and therapeutic evaluation of RAS-GTP inhibition by RMC-6236 in RAS-driven cancers. *Cancer Discov.* **14**, 994–1017 (2024).
37. Cereda, M. et al. Patients with genetically heterogeneous synchronous colorectal cancer carry rare damaging germline mutations in immune-related genes. *Nat. Commun.* **7**, 12072 (2016).
38. Morandi, E. et al. HaTSPiL: a modular pipeline for high throughput sequencing data analysis. *PLoS ONE* **14**, e0222512 (2019).

39. Cibulskis, K. et al. Sensitive detection of somatic point mutations in impure and heterogeneous cancer samples. *Nat. Biotechnol.* **31**, 213–219 (2013).
40. Saunders, C. T. et al. Strelka: accurate somatic small-variant calling from sequenced tumor-normal sample pairs. *Bioinformatics* **28**, 1811–1817 (2012).
41. Koboldt, D. C. et al. VarScan 2: somatic mutation and copy number alteration discovery in cancer by exome sequencing. *Genome Res.* **22**, 568–576 (2012).
42. Favero, F. et al. Sequenza: allele-specific copy number and mutation profiles from tumor sequencing data. *Ann. Oncol.* **26**, 64–70 (2015).
43. D'Aurizio, R. et al. Enhanced copy number variants detection from whole-exome sequencing data using EXCAVATOR2. *Nucleic Acids Res.* **44**, e154 (2016).
44. Frankish, A. et al. GENCODE reference annotation for the human and mouse genomes. *Nucleic Acids Res.* **47**, D766–D773 (2019).
45. Wang, K., Li, M. & Hakonarson, H. ANNOVAR: functional annotation of genetic variants from high-throughput sequencing data. *Nucleic Acids Res.* **38**, e164 (2010).
46. Repana, D. et al. The Network of Cancer Genes (NCG): a comprehensive catalogue of known and candidate cancer genes from cancer sequencing screens. *Genome Biol.* **20**, 1 (2019).
47. Melloni, G. E. M. et al. Precision Trial Drawer, a Computational Tool to Assist Planning of Genomics-Driven Trials in Oncology. *JCO Precis Oncol.* **2**, 1–16 (2018).
48. Li, Q. et al. CancerVar: An artificial intelligence-empowered platform for clinical interpretation of somatic mutations in cancer. *Sci. Adv.* **8**, eabj1624 (2022).
49. Li, M. M. et al. Standards and Guidelines for the Interpretation and Reporting of Sequence Variants in Cancer: A Joint Consensus Recommendation of the Association for Molecular Pathology, American Society of Clinical Oncology, and College of American Pathologists. *J. Mol. Diagn.* **19**, 4–23 (2017).
50. Roth, A. et al. PyClone: statistical inference of clonal population structure in cancer. *Nat. Methods* **11**, 396–398 (2014).
51. Dang, H. X. et al. ClonEvol: clonal ordering and visualization in cancer sequencing. *Ann. Oncol.* **28**, 3076–3082 (2017).
52. Del Giudice, M. et al. FOXA1 regulates alternative splicing in prostate cancer. *Cell Rep.* **40**, 111404 (2022).
53. Meng, P. et al. Detecting therapy-guiding RNA aberrations in platelets of non-small cell lung cancer patients. Preprint at medRxiv https://doi.org/10.1101/2021.01.26.21250013 (2021).
54. Ng, P. K. S. et al. Systematic functional annotation of somatic mutations in cancer. *Cancer Cell* **33**, 450–462.e10 (2018).
55. Siswanto, F. M., Oguro, A. & Imaoka, S. Sp1 is a substrate of Keap1 and regulates the activity of CRL4AWDR23 ubiquitin ligase toward Nrf2. *J. Biol. Chem.* **296**, 100704 (2021).
56. Ianevski, A., Giri, A. & Aittokallio, T. SynergyFinder 3.0: an interactive analysis and consensus interpretation of multi-drug synergies across multiple samples. *Nucleic Acids Res.* **50**, 739–743 (2022).
57. Yadav, B., Wennerberg, K., Aittokallio, T. & Tang, J. Searching for drug synergy in complex dose-response landscapes using an interaction potency model. *Comput. Struct. Biotechnol. J.* **13**, 504–513 (2015).
58. Di Veroli, G. Y. et al. Combenefit: an interactive platform for the analysis and visualization of drug combinations. *Bioinformatics* **32**, 2866–2868 (2016).


## Acknowledgements

We are grateful to Sara Cano and Eduard Batlle (IRB, Barcelona, Spain) for helpful advice on the analysis of TGFB signaling. We are indebted to Matthew Holderfield, David P. Wildes, Jacqueline A. Smith, and Steven Kelsey from Revolution Medicines for providing the RMC-4998 compound and for insightful discussions. This work was funded by grants from Institut National du Cancer (grant No. INCA_13911), SIRIC-BRIO (Bordeaux Recherche Intégrée en Cancérologie, INCa convention 2018-006 & INSERM convention 18CI05500), the French government in the framework of the Investments for the Future program IdEx-Université de Bordeaux, Ministerio de Ciencia e Innovación (PID2020-116824RB-I00) and Scientific Foundation of the Spanish Association Against Cancer (EPAEC222641CICS and PRYGN222960SANT) (to D.S.), the Giovanni Armenise–Harvard Foundation, the Italian Ministry of University and Research (FARE-R207ENY9KZ), the European Research Council (ERC) under the European Union's Horizon 2020 research and innovation program (grant agreement No. [101001288]), AIRC under IG 2021—ID. 25737 project and Revolution Medicines under a sponsored research agreement (to C.A.), Instituto de Salud Carlos III (grant PI21/00789) (co-funded by European Regional Development Fund, ERDF, a way to build Europe) (to E.N.) and two grants from the Spanish Ministry of Economy and Competitiveness - Instituto de Salud Carlos III FEDER (PI21/00789 and FIS PI22-00548), Generalitat de Catalunya 2021SGR00184 (to E.N. and A.V., respectively). M.J.N. was supported by a bourse d'excellence de la Fédération Wallonie-Bruxelles (WBI) and a postdoctoral fellowship from Foundation ARC pour la recherche contre le cancer. B.R. was supported by the Barbara Gomez Endowed Advanced Program in Thoracic Oncology. D.A.-V. held a PFIS predoctoral fellowship (FI20/00130) from Instituto de Salud Carlos III. M.C. is supported by AIRC under MFAG 2017—ID. 20566 and BRIDGE 2023—ID. 28739 projects and the Compagnia di San Paolo Foundation. C.A. is supported by the Zanon di Valgiurata family through Justus s.s.

## Author contributions

M.J.N., A.M., M.C., D.S., and C.A. conceived this project and designed the study. M.J.N., A.M., E.P., B.R., S.C., I.S., S.S.J., S.P., L.C., S.V.M., A.B., X.W., D.A.-V., M.M.-I., Au.V., T.R., C.G.-M., A.V., and M.C. performed the experiments and analyzed the data. S.C., I.S., M.M.A., E.N., and A.I. provided materials, methodological support and/or conceptual advice. M.-J.N., A.M., B.R., M.C., D.S., and C.A. wrote the manuscript. All authors discussed the results and commented on the manuscript.

## Competing interests

The authors declare the following competing interests: D.S. received research fees from Aelin Therapeutics. C.A. received research fees from Revolution Medicines, Aelin Therapeutics, Verastem, Roche, and Boehringer Ingelheim. A.I. received research support from AstraZeneca, Bayer, BMS, Merck, MSD, Pharmamar, and Roche and participated as a consultant in advisory boards for Bayer, Blueprint, Daiichi Sankyo, Epizyme, Fstar Therapeutics, Roche and Springworks. S.C. participated as a consultant on advisory boards for Roche, BMS, and AstraZeneca. B.R. received advisory board/consulting and honoraria fees from AstraZeneca, Regeneron, Amgen, Bayer, SITC, and Targeted Oncology. M.M.A. received advisory board/consulting and research fees from Merck, Pfizer, Bristol Myers Squibb, Foundation Medicine, Novartis, Gritstone Bio, Mirati Therapeutics, EMD Serono, AstraZeneca, Instil Bio, Regeneron, Janssen, Affini-T Therapeutics, Genentech/Roche, Lilly, Amgen. E.N. received research support from Roche, Pfizer, Bristol Myers Squibb and Merck Serono and participated as consultant in advisory boards for Amgen, AstraZeneca, Bayer, Boehringer Ingelheim, Bristol Myers Squibb, Daiichi Sankyo, Janssen, Lilly, Merck Serono, Merck Sharpe & Dohme, Pfizer, Roche, Sanofi and Takeda. E.N. participated as an investigator of clinical trials from Amgen and Revolution Medicines related to the current publication. Au.V. and A.V. are founders of the spin-off Xenopat S.L. The remaining authors declare no competing interests.

## Additional information

**Supplementary information** The online version contains supplementary material available at https://doi.org/10.1038/s41467-024-51828-2.

**Correspondence** and requests for materials should be addressed to Antoine Italiano, Matteo Cereda, David Santamaría or Chiara Ambrogio.

**Peer review information** *Nature Communications* thanks John Minna, and the other, anonymous, reviewer(s) for their contribution to the peer review of this work. A peer review file is available.